

ENMA490

5/10/2013

Team H₂ Final Report

Photocatalytic Water Splitting Using ZnWO₄ and NiO_x Catalysts



Norena Beaty
Nicholas Faenza
Tanner Hamann
Owen McGovern
Santiago Miret
Mark Reese

Abstract

Photocatalytic materials are a promising method for producing clean hydrogen. However, current photocatalytic systems involve expensive materials, cannot be scaled up to an industrial level, or suffer from low efficiencies. This study explores a novel combination of ZnWO_4 and NiO_x catalysts, which are both inexpensive and also require nothing more than basic fabrication procedures. Our team designed a photocatalytic system with 400-500 nm ZnWO_4 nanoparticles with 1-2 wt% of NiO_x co-catalysts to achieve maximum productivity. Design factors such as size, crystallinity, surface area, and composition were investigated to improve photocatalytic performance. Preparation of the samples involved wet chemistry and calcination in a box furnace at temperatures not exceeding 500 C. Samples were successfully fabricated and characterized with X-Ray Diffraction (XRD), Scanning Electron Microscopy (SEM), particle size analysis and other characterization techniques. The results of the characterization were used to modify the fabrication procedure with the aim of getting our parameters to match our design targets. We also applied density functional theory (DFT) calculations to conduct preliminary relaxations of NiO_x and ZnWO_4 crystals as a precursor to calculating bulk band structures for both materials. While the performance of the photocatalytic system is inconclusive due to time constraints, a strong foundation of research and a fully designed system was achieved. We also used kinetic Monte Carlo (KMC) simulations to study the formation of the NiO_x co-catalyst with the goal of adjusting our fabrication procedure based on the simulation results. This project demonstrated the successful fabrication of a low cost photocatalytic system, and designed an optimized prototype. To our knowledge, this project was the first to show deposition of NiO_x on a ZnWO_4 substrate.

Project Summary

Motivation

Sustainability initiatives have spread into most, if not all, aspects of modern society as seen in the recycling of paper, plastic, and metal products, the construction of more energy efficient buildings, and the search for viable alternative fuels for automobiles ^[11]. Perhaps one of the most important current sustainability efforts is the construction of clean energy systems. The demand for electricity is increasing with the growing global population and the spread of easily accessible technology products that require energy. The most used methods of energy production, including coal, natural gas, and nuclear are all energy systems that generate large amounts of greenhouse gases or toxic waste products ^[8]. To meet the energy challenge, one has to engineer a clean energy system that is technologically and economically competitive with current energy infrastructure systems with little or no environmentally dangerous byproducts. Our project focuses on photocatalytic water splitting, by which absorbed photons generate electrons inside a material that can reduce hydrogen from an aqueous solution. Hydrogen gas contains about three times the energy density of natural gas, produces only water when burned, and could serve as a fuel source for fuel cells automobiles, thereby addressing another significant CO₂ emission source. Furthermore, photocatalytic water splitting is an easily scalable process, making it more viable as a supply of hydrogen. Theoretically, photocatalytic water splitting is a technically viable, ^[1] and economically feasible ^[1] clean energy harvesting process, however current systems do not employ effective photocatalyst materials. Current catalyst systems often employ inefficient materials or involve the use of expensive rare-earth minerals ^[1]. Our project aims to address this problem by designing and testing the viability of a ZnWO₄ photocatalyst with a NiO_x co-catalyst.

Intellectual Merit

We gained a number of insights by conducting this project. The first is an overarching understanding of how the structure of the material affects the chemical properties. We accomplished this through analysis of various parameters of the material structure, including the physical lattice structure, the surface structure and the sites of reacting electrons. Understanding the physical structure of the material allowed us to minimize the amount of electron-hole pair recombination in the material. We minimized the number of electron-hole recombination sites in the materials by reducing the number of material defects and decreasing the distance the electrons and holes have to travel. We also determined how our designed material structure and resulting properties affects the material performance as measured by our design parameters.

Project Impact

Developing an effective and inexpensive photocatalytic system represents a tremendous breakthrough in economic and environmentally friendly hydrogen production and energy generation. Hydrogen is advantageous because of its relatively high energy

density, storage capacity and its environmentally sustainable nature. Assuming that hydrogen is burned in a pure oxygen environment, the primary emission would be water vapor and no greenhouse gases or other pollutants. Photocatalysts also represent a cleaner method of producing hydrogen, instead of current chemical and industrial processes that rely on fossil fuels. Hydrogen is currently produced by steam reforming from fossil fuel refined hydrocarbons and electrolysis^[11], resulting in the release of greenhouse gases such as CO and CO₂. Past and current research efforts^[1] have also investigated hydrogen production by electrolysis. Electrolysis, however, is a very energy inefficient process^[16]. Photocatalysts would allow hydrogen production from solar energy and the abundant supply of water found on earth.

The societal impact of successful implementation of this technology would be substantial. Photocatalytic water splitting would enable large-scale production of hydrogen as a primary fuel for transportation, heating, and electricity, as well as numerous chemical processes. Widespread hydrogen use would drastically reduce the emission of greenhouse gasses, and thereby have positive effects on the environment. Hydrogen is also widely used throughout industrial processes, and access to cheap, clean hydrogen would be beneficial for the chemical industry as well. While there are other hydrogen technologies, such as storage, that need to be addressed^[17], photocatalytic water splitting could have a profound impact on hydrogen production and be the foundation for future energy and chemistry innovations.

Materials Science and Engineering Aspect

Designing the photocatalytic system of ZnWO₄ and NiO_x involved an understanding and application of a plethora of Materials Science and Engineering (MSE) aspects. The applicable MSE aspects of this project can be broken down into four sections; the electronic band structure, Ni oxidation, characterization, and the impact of material properties on the particle's performance. DFT simulations were done to understand the electronic band structure of our system. To write and run these simulations, a strong understanding of atomic interactions, crystal structure, and relevant material properties was necessary. For example, knowledge of both the ZnWO₄ and NiO_x crystal structure as well as the electron states of each material was required to model how excited electrons will flow from phase to the other. It was also crucial to understand exactly how the crystal faces of each material aligned during contact. The properties previously stated have many direct ties to MSE lessons, and running the simulations would not be possible without an understanding of these properties.

Kinetic Monte Carlo (KMC) simulations were also employed to better understand the formation of the NiO_x nanoparticle via oxidation of deposited nickel. The simulation calculated the probability of various chemical and diffusion processes for a particle atom/molecule, based on the different rate constant for each process and the surrounding conditions. Determining the rate constants required concepts from kinetics, thermodynamics and basic materials science, such as activation energy barriers, bond disruption/formation, lattice structure, vacancy concentrations, and collision theory. The integrity of the simulation and reliability of the results depended on how well the various real-world processes and effects were accounted for when selecting which process to execute.

The performance of our particles is highly dependent on its material properties, as well as the properties that our team designed. While the materials were specifically chosen for their enhanced characteristics, it took an in-depth understanding of how the designed parameters affected the system's performance to reach a final design. An example of this would be how our design tried to maximize the crystallinity to reduce the number of grain boundaries, which act as recombination centers for the excited electron hole pairs. At the same time our design wanted to enhance the surface area, which adds more reaction sites, however, surface area and crystallinity are competing processes. Understanding crystal growth mechanism allowed us to determine the fabrication parameters that would provide us with an optimal balance of crystallinity, size and surface area. Crystal growth, and the fabrication methods that we used are common aspects of MSE, and have been consistently reinforced during our undergraduate education.

In order to gain insight into what the fabrication process actually produced, various forms of characterization played a critical role. XRD provided information on the crystallinity, and composition of the particles, while SEM gave a visual, which showed the relative size, shape, and uniformity. Furthermore, a particle size analyzer released a distribution of our particle sizes, which was crucial for understanding if our particles were single crystals or agglomerates. The three techniques previously mentioned are common characterization techniques used in MSE. In order to successfully analyze the data from these techniques an understanding of the testing mechanisms and relevant material properties are necessary, which has a direct correlation to MSE aspects.

Design Goals

This project was aimed at developing a cost efficient photocatalytic system for water splitting. The aim was pursued by designing a system with a new combination of materials, and then comparing these results to similar studies. Specific design goals for this project include using density functional theory to model the band structure of ZnWO_4 and NiO_x , creating kinetic Monte Carlo simulations to understand the effect of annealing time and temperature on the oxidation of nickel, and optimizing system parameters such as size, crystallinity, and surface area to improve performance. Beyond the design stage, our team aimed to successfully fabricate our system, and then test the water splitting capabilities of our particles. Lastly, a comparison was to be drawn between our results and goals, to those of similar studies.

Ethics and Environmental Impact

One important consideration in our project is our use of nanoparticles, for which the health implications are not yet well understood. In the lab it is relatively simple to seal the particles so that they cannot contaminate the air and cause harm to their surroundings. However, it is possible that if used in a large-scale facility, a fair quantity of nanoparticles could escape from the system and be inhaled. The facility would have to be designed with this consideration in mind.

We are also placing emphasis on the use of safe materials. For our project in particular, we are avoiding the use of lead. Lead is toxic and can cause various health

problems such as damage to the nervous system or brain ^[22]. Due to the risks involved in the use of lead, we used ZnWO_4 instead of PbWO_4 . The co-catalyst used throughout this project was NiO_x . While nickel is slightly toxic, the volumes of Ni used for our purpose should lead to little risk. Even if the process reaches an industrial scale, the amount of nickel in each nanoparticle is minimal, making the toxicity a minor problem unless large volumes of the powder are inhaled.

Another potential ethical issue involves the flammability of hydrogen gas, which can be dangerous, especially when hydrogen is stored in large pure quantities. Since our project is intended to create hydrogen from water, the storage and handling of the gas are very important. In a laboratory setting, it is unlikely that large volumes of hydrogen gas will be produced, thereby reducing this risk for our project. However, if the process is performed on an industrial scale, this risk can quickly become significant. These risks have been known and mitigated by the chemical industry for a prolonged period of time. Hydrogen is already being stored in large quantities today in spite of these risks and our hydrogen production procedure is compatible with these risks.

In spite of the aforementioned risks, the benefits of the project outweigh its weaknesses. If a cost effective photocatalytic system can be developed, the benefit to humanity would be substantial. Burning dirty fossil fuels has a plethora of ethical and environmental setbacks including, air contaminants, greenhouse gases, and the destruction of multiple ecosystems. Replacing fossil fuels with hydrogen produced by water splitting will eliminate or severely mitigate these consequences, which in turn makes photocatalysis very ethical and environmentally friendly on an industrial level. The research proposed and conducted holds small amounts of risk but may contribute to a globally important development. As a result the anticipated conclusions of this project are not only ethical but would have a drastic positive impact on the environment and atmosphere.

Technical Approach

Team H2 utilized simulations and a careful review of the literature to develop an effective design to our ZnWO_4 and NiO_x photocatalytic system. From our design we synthesized the particles, fabricated a prototype photocatalytic system, and started to measure its properties.

Simulations

In order to successfully design a photocatalytic water splitting system successfully, Density Functional Theory (DFT) calculations of our materials were necessary. From the DFT calculations of ZnWO_4 and NiO_x , our group expected to gain an in-depth understanding of the electronic band gap and band edge placements of the photocatalytic materials, as well as the light absorption mechanisms of the system ^{[4][5]}. Knowledge of the ZnWO_4 and NiO_x band structures would help us determine the optimal composition and structure of each material. Our system utilized a Z-scheme system where two photocatalysts are employed, one for the oxidation reaction and one for the reduction reaction ^[1]. It was therefore important that we modeled the electronic structure of both photocatalysts.

Using the DFT modeling, our group intended to tune the properties of the oxide materials to maximize the UV absorption and preserve the potential redox reactivity^[12]. Maximizing the UV absorption is especially important since it comprises only a few percent of the solar spectrum. This severely restricts the number of photons that can be absorbed to create optically excited states and, subsequently, charge carriers needed for the redox chemistry^[12].

Considering this particular Z-scheme system of NiO and ZnWO₄ has not been synthesized before this point, the results from the DFT calculations we planned for this project would have a direct effect on the synthesis procedure. We theorized that the angle of adsorption of the NiO particle on the larger ZnWO₄ particle would affect the band gaps and therefore structure of the system. DFT surface simulations and VASP specifically were ideal for calculating band gap as a function of contact angle considering that *ab initio* calculations are highly scalable and can handle large amounts of data^[21]. Meanwhile, DFT bulk calculations are used to compute the band edge alignments of solid-solid interfaces, such as the one between ZnWO₄ and NiO^[21]. This alignment would change depending on the internal composition of NiO, which our group also theorized may not be entirely composed of NiO as we originally assumed. Therefore, the DFT calculations for the band gap and band edge placement would have an impact on the prototyping stage since they would ideally show what compositions and angle of adsorption would maximize the UV absorption of the system.

As part of designing the nanoparticles, we planned to run KMC simulations to study the formation of the NiO_x co-catalyst via oxidation of nickel initially deposited onto the ZnWO₄^[18]. As a result, we gained a better understanding of the internal composition of the NiO_x co-catalyst. We also studied how varying certain material parameters, such as contact angle and oxidation time, changed the composition. Ideally, we wanted nanoparticles composed of 100% NiO^[6], and the simulation could be applied to determine the optimum synthesis conditions. Alternatively, we could measure our fabricated nanoparticles to determine the input parameters, then model the NiO to complement the spectroscopy techniques. The simulation considered adsorption, diffusion, and chemical reactions to account for the various processes present during oxidation.

Synthesis

The synthesis of our system occurs in two stages. First, we fabricate the ZnWO₄ particles using a calcination process. Following the synthesis of the ZnWO₄ nanoparticles, we deposit the NiO_x co-catalyst on the ZnWO₄ particles. The starting materials of the ZnWO₄ synthesis are Zn(NO₃)₂ * 6H₂O and Na₂WO₄ * 2H₂O in a 1:0.7 molar ratio^[4, 8]. Upon mixing a white precipitates start forming immediately, but we use sonication for 30 min to ensure complete reaction of the precursors. Following sonication, the precipitates are filtered, washed with ethanol, and dried in air at 85 °C^[8]. Once the powder is fully dry the sample is calcined in a box furnace at 500 °C for 4 hours in air^[8]. We calcined the sample in a 50 mL alumina crucible, because at the relatively low temperature of 500 °C the zinc, nickel, and sodium will not contaminate the furnace. The above procedure was determined from extensive literature review and created ZnWO₄ nanocrystals that are 300-400 nm in diameter^[1, 4, 7, 8].

After the calcination process is complete, we deposited Ni onto the ZnWO₄ nanoparticles. We used a NiO_x content ranging from 1-2 wt% for our catalyst system. The NiO_x particles are deposited by mixing Ni(NO₃)₂ * 6H₂O with the particles in DI water and then kept at 80 °C until fully dry. The powder is then placed in an alumina crucible and calcined in air at 350 °C for 1 hour to oxidize the Ni ^[1, 2, 6]. The target particle size of the NiO_x co-catalyst particles was on the order of 12 nm, but appeared to be closer to 40 or 50 nm ^[20]. This process concludes our synthesis procedure, rendering our particles ready for characterization and performance testing.

Characterization

We plan on applying a variety of characterization methods to analyze our sample structure and properties. Our primary characterization methods include scanning electron microscopy (SEM), X-ray diffraction (XRD), a particle size analysis based on light absorption measurements in a dispersed particle solution. If possible, we would also like to measure the surface area of our particles using Brunauer-Emmett-Teller (BET) measurements. The SEM will provide detailed images of our nanoparticles and enable us to perceive the relative size, shape, and distribution of our crystals. This process allows us to assess the merit of our procedure and determine if we achieved our desired structure. With the SEM we will also be measuring the contact angle of our NiO_x particles, which is necessary for our simulation efforts. XRD will provide valuable insight into the crystallinity and lattice structure of our particles, which are important for estimating recombination, and confirming many of our simulation assumptions like a monoclinic wolframite crystal structure. BET calculations are important to determine the surface area of the particles, which has been found to have a very strong correlation to the photocatalytic efficiency ^[7]. Lastly, the Zetasizer Nano particle size analyzer will provide supporting results our particle size distribution (PSD). This is necessary because the particle size is also critically important to the systems functionality. We plan on conducting some of these characterization methods, including SEM, PSD, and XRD on the ZnWO₄ samples prior to the deposition of NiO_x, in order to ensure that the effectiveness of our initial fabrication. Following NiO_x deposition, we will apply the same characterization techniques to assess the effectiveness of our NiO_x fabrication process and to characterize our final product in a relatively comprehensive manner.

We plan on conducting performance measurements in addition to the characterization methods stated in order to further understand the functionality of our system. The performance testing will consist of submerging our particles in water, irradiating the system with the solar simulator that is in the university FabLab. Given time and budgetary constraints, the performance testing will be qualitatively focused and used mainly as a proof of concept for our design. Measurement of H₂ and O₂ produce would require the use of a gas chromatograph setup, which may not be feasible within the scope of the project. Following the solar simulator, we would like to conduct the UV lamp test if time and resources permit. We will employ multiple characterization and performance testing techniques to develop a complete understanding of our particles properties as well as its functionality.

Summary

In conclusion, team H2 will be prototyping a photocatalytic system for water splitting using a $\text{ZnWO}_4/\text{NiO}_x$ catalyst. The catalyst will be fabricated from calcination and solution processes to form 400-500 nm particles with roughly a 10 nm co-catalyst. The sample will be extensively characterized with SEM, XRD, BET, and a particle size analysis to obtain an in-depth understanding of our crystals properties. The performance of our system will be tested in a proof of concept test by irradiating the samples with solar simulator. The final prototype should include successfully fabricated $\text{ZnWO}_4/\text{NiO}_x$ particles submerged in water and tested for its water splitting capabilities.

Prototype

Design

We designed our materials, composition, and structure parameters to maximize the photocatalytic capabilities of the catalyst system. Our principal design parameters included particle size, crystal structure, and surface area. Since these parameters can be changed through variations in the fabrication procedure, we conducted a thorough review of the literature to understand how different synthesis methods affect the material characteristics. We aimed to achieve the highest possible crystallinity for the ZnWO_4 and NiO_x nanoparticles to reduce the number of recombination sites, and thereby maximize the efficiency of our system. We found ZnWO_4 reaches favorable crystallinity when the calcination temperature is 500 °C or higher^[1,8]. Annealing at higher temperatures for this synthesis is disadvantageous because annealing will provide sufficient energy to overcome the activation energy barrier necessary for necking between particles to occur, thus resulting in a larger particle size. Calcination at higher temperatures also reduces the surface area, which limits the number of reaction sites, and impedes efficiency^[8]. For the above reasons, our team decided to anneal at 500 °C, so that we can obtain high crystallinity without sacrificing the surface area of our nanoparticles. All of the calcination processes for this project were done in a low temperature box furnace.

The calcination time also has a profound impact on particle structure, even though its effect has been found to be less important than the calcination temperature^[4]. Previous studies have found that the longer the annealing duration, the higher the crystallinity becomes, and the lower surface area obtained^[8]. The relationship between the surface area and calcination parameters is shown in the following figures:

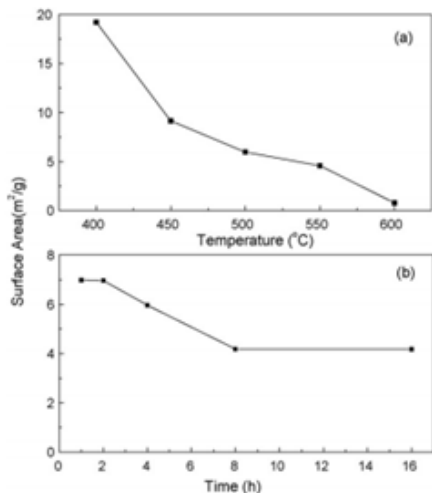


Figure 1: Relationship between the surface area of ZnWO₄ particles and the calcination parameters (4 hours for 1 a and 500 C for 1 b).^[8]

Optimal photocatalytic performance is achieved with a good balance between crystallinity and surface area, due to the competing nature of these processes^[8]. A previous experiment with a ZnWO₄ catalyst^[8] shows that the optimal photocatalytic efficiency is achieved at a calcination temperature of 500 °C and an annealing time of 4 hours. This graph is shown in Figure 2 below. The results of the study have prompted our group to adopt the fabrication parameters for our design.

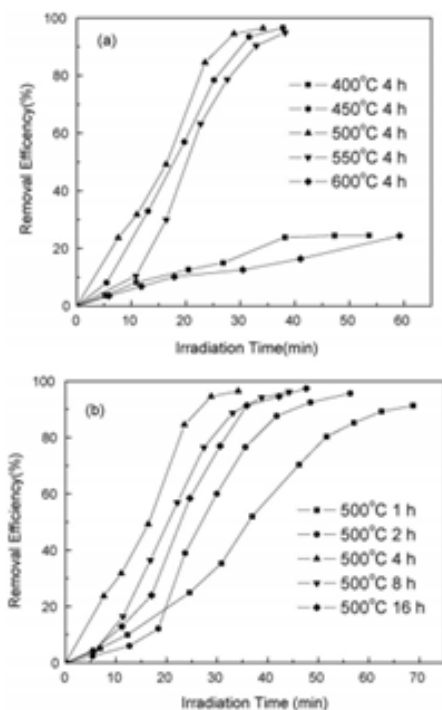


Figure 2: Effects of calcination temperature and time on the photocatalytic properties of ZnWO₄.^[8]

Understanding the crystal structure of ZnWO_4 is important for understanding the optical and electrical properties of the material. Our group will be fabricating ZnWO_4 in the monoclinic wolframite crystal structure. This structure is the principal crystal structure for ZnWO_4 and is stable up to 1486 K and 39 GPa^[13]. Since neither our processing parameters nor our testing environment will create conditions remotely close to the given temperature and pressure (1486 K and 39 GPa respectively) we can be confident that our structure will be in the monoclinic wolframite phase. Our assumption is also supported by test results from past studies^[4,7,8].

Our technical approach includes details on the fabrication of the NiO_x co-catalyst. The Ni co-catalyst material will be synthesized in a solution-based reaction, and will then be oxidized in air to form the NiO_x particles^[6]. This method of depositing the NiO_x particles was chosen because of its capability to control the particle size. We also have the ability to control the particle for ZnWO_4 by varying the temperature and time parameters of our synthesis method^[2]. The particle size of NiO_x particles can also be modified by varying the concentration of the solution for the deposition of the Ni. In this case, a higher concentration of Ni will correspond to larger particles^[1,6]. Previous studies suggest that NiO_x particles with a size of 12 nm and a 1.0 wt% in the catalyst system of $\text{ZnWO}_4 / \text{NiO}_x$ yields the best results^[20]. At this moment, we aim to use 1.0 wt% NiO_x in our catalyst system given the results in the literature. The weight percent may be adjusted based on our future experimental measurements of our final catalyst system. The previously stated parameters constitute our finalized design. The drawing shown in Figure 3 below shows a schematic of how we aim to arrange our catalyst system. The drawing assumes a contact angle of 90° between the ZnWO_4 and the NiO_x . The literature review yielded no measurement of contact angles in previous studies and the 90° was assumed to enable calculations and simulations that will be described later in the study.

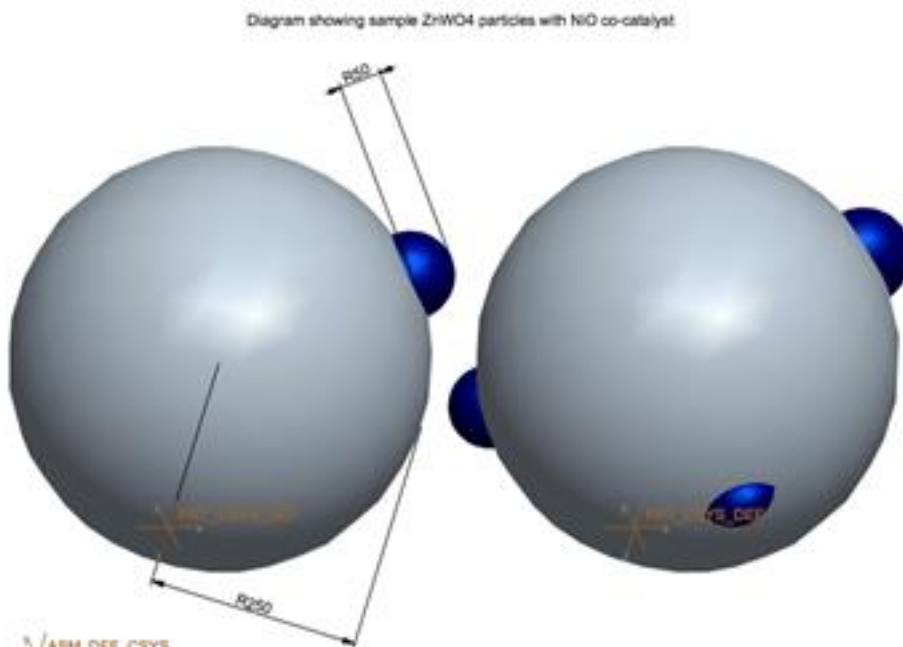


Figure 3: Schematic drawing of catalyst structure; ZnWO_4 (grey) and NiO_x (blue); radii are in nanometers (Spherical Shape and 90° contact angle assumed).

Facilities and Materials

Successful completion of our design and prototype required various instruments, materials, and laboratories across the University of Maryland campus. Access to a scanning electron microscope (SEM), x-ray diffractometer (XRD), and particle size analyzer are necessary for characterization of our particles. We accessed the NISP lab to analyze our particles with an SEM. In order to perform XRD, we have used the University of Maryland's X-ray Crystallographic Center. To determine the size distribution of our particles we tested our samples on the Zetasizer Nano located in the Kim Engineering Building Teaching Lab. The precursors purchased were zinc nitrate hexahydrate, nickel (II) nitrate, and sodium tungstate. Laboratory space and a box furnace were needed for fabrication of our crystals, and an additional laboratory was needed to test the performance of our photocatalytic system. Dr. Rabin has graciously allowed us to use his lab for the ZnWO_4 synthesis and the deposition of Ni on our ZnWO_4 powder. For all of our calcination steps we used Dr. Wachsmann's low temperature box furnace. We conducted all of our performance testing using the Solar Simulator in the University of Maryland FabLab.

As mentioned previously in the *Simulations* section, access to VASP, as well as the computing power of XSEDE was made available by Professor Einstein. The VASP files and the XSEDE supercomputers were necessary to complete the DFT calculations for ZnWO_4 and NiO. Professor Einstein and his graduate student, Josue Morales have graciously helped us with using the VASP package and obtaining computing time from XSEDE. The kinetic Monte Carlo simulations were done through MatLab on our personal computers.

Summary of Performed Work

Our team's modeling efforts were significantly adjusted based on a better understanding of our system and our limitations in performing calculations using DFT due to time constraints and incipient understanding of VASP. While the scope of our DFT calculations was curtailed to a simpler effort to determine band structure, we expanded modeling efforts to investigate the processes of nickel and subsequent nickel oxide formation using the kinetic Monte Carlo (KMC) method within the Matlab programming environment. These processes were subdivided into adsorption, diffusion, and reaction steps that were handled by the probabilistic Monte Carlo method. Multiple relaxations using DFT were completed to establish the stable unit cell dimensions and atomic positions from the already attained crystal structure and experimental unit cell data, and a qualitative depiction of two dimensional diffusion of nickel and oxygen atoms was achieved using KMC, and expanded to three dimensions. There are other considerations that were factored into KMC modeling in order to produce a more accurate picture of kinetic processes, including literature-based rates of individual processes (e.g. oxygen reaction with nickel) and a treatment of reacted nickel oxide particles.

Significant work was completed on the fabrication side of the project: two batches of ZnWO_4 were prepared using our synthesis procedure. The first was plentiful enough for beginning characterization, such as XRD and particle size analysis, but the second

sample was produced with the intent of depositing NiO_x, in order to finalize the photocatalytic system.

Characterizations performed included XRD and particle size analysis. We also performed SEM characterization. XRD data has shown that we have produced high crystallinity monoclinic wolframite zinc tungstate, affirming our fabrication process. One issue that was unresolved was possible agglomeration of particles as indicated by particle size analysis. With additional time, further adjustments to the fabrication process would be made to address this problem.

Simulations: DFT

After consulting with Dr. Einstein, we were introduced to one of the grad students in his group, Josue Morales, who had extensive experience in using the Vienna Ab-initio Simulation Package (VASP), which performs Ab-initio quantum mechanical molecular dynamics using DFT calculations. Since the last quarter report, the Simulations team met multiple times with Josue in order to get his advice and guidance in terms of the steps necessary to arrive at a band gap calculation using VASP.

Due to the fact that a single photocatalyst particle had far too many atoms to reasonably model using VASP, the scope of our calculations was reduced without sacrificing our overall goal of determining the band structure of the materials. Josue instead suggested that our group attempt to model simply the surface and therefore the interaction between the two crystal structures of ZnWO₄ and NiO_x. This surface calculation would theoretically allow us to see how adsorption angle of the NiO_x particles on ZnWO₄ would affect the band gap/band edge positions. In order to perform such a simulation, knowledge of the surface structure of both particles and how the crystal structure of ZnWO₄ and NiO_x interacted at the surface were required.

Josue introduced our group to an open software called Visualization for Electronic Structural Analysis (VESTA) that helped us visualize the crystal structures and how they would fit together. The crystal structure data for ZnWO₄ and NiO_x such as fractional coordinates for the atoms, unit cell lengths, etc. were obtained from Materials Project, a website that catalogues the structural information of various materials. Our group was able to create the crystal structures for ZnWO₄ and NiO_x, Figure 4 and Figure 5 respectively, though the bond lengths in the unit cells were assumed not entirely correct for the photocatalytic system.

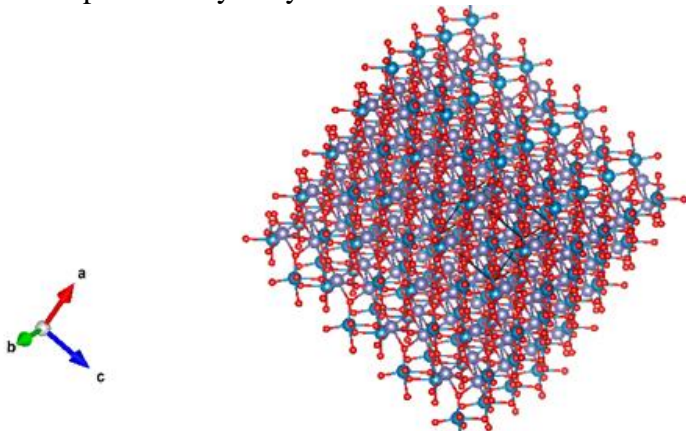


Figure 4: The VESTA simulation of a ZnWO₄ crystal lattice.

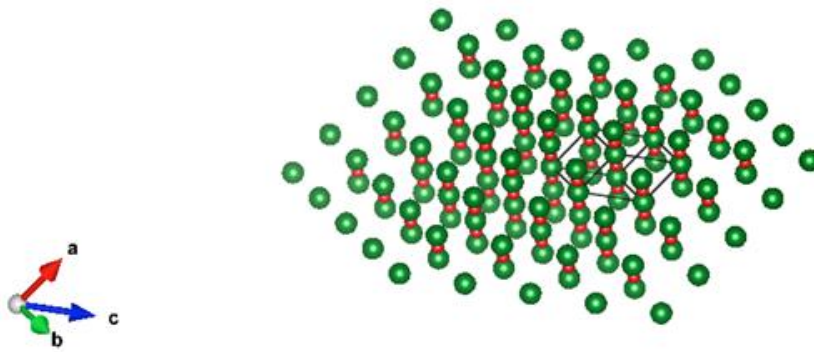


Figure 5: The VESTA simulation of a NiO_x crystal lattice.

Our group recently consulted with a visiting professor from the Massachusetts Institute of Technology (MIT), Yifei Mo, whose research often involves the use of DFT calculations and software. Upon explaining our current project goals to Professor Mo, he advised that the surface calculations were too intensive for the amount of time left and advised that the band structure be computed using a bulk calculation instead. He also provided several papers concerning how one can obtain a more accurate band gap from simple DFT calculations, how to screen materials computationally for water catalysis, and the methodology to evaluate band alignment at the catalyst/co-catalyst interfaces. Our group proceeded to carry out the steps necessary to perform bulk calculations on the two materials to obtain their band structures. This was done by running several relaxation calculations on the unit cells so that the configuration with the lowest energy (and therefore the most likely cell size and bond lengths) were obtained. The resulting energy minimization plots can be seen below in Figure 6:

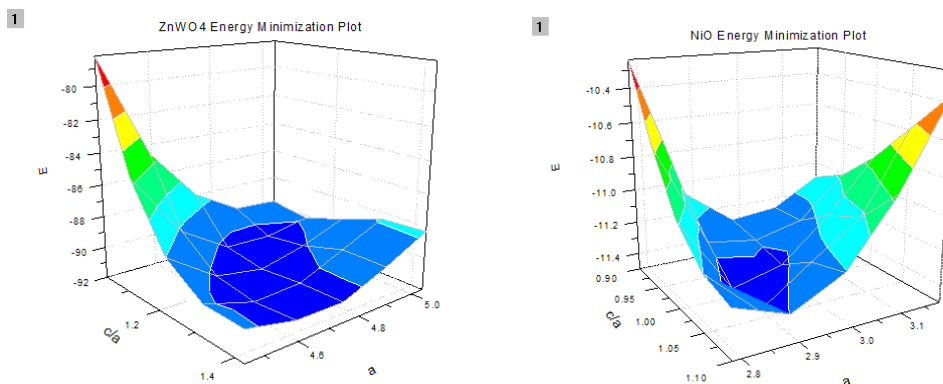


Figure 6: The energy spread of 25 different ZnWO_4 (right) and NiO (left) cell configurations, respectively.

Simulations: KMC

The formation of the nickel (II) oxide (NiO) nanoparticles via oxidation of nickel previously deposited on the ZnWO_4 particle at $300\text{ }^\circ\text{C}$ was modeled using a KMC simulation. The basis for the processes involved in NiO formation and included in the

simulation is presented in Figure 7.^[36] Molecular oxygen initially impinges on the nickel surface and adheres, after which the molecular oxygen dissociates in two atomic oxygen.^[36] The layer of surface atomic oxygen builds over time until reaching a critical value at which NiO islands nucleate and begin to grow outwards.^[36] The islands coalesce into a continuous surface layer of NiO that proceeds to grow into the nickel bulk.^[36] As such, the simulation included nickel atoms in a face-centered cubic (FCC) lattice, molecular oxygen that adhered to the surface, and atomic oxygen that diffused across the surface and the bulk as well as reacted with neighboring nickel to form NiO. For coding simplicity, these three species were further differentiated into molecular oxygen in air, adsorbed molecular oxygen, atomic oxygen, bonded atomic oxygen, nickel atoms in FCC, and bonded nickel. Vacancies were also included to establish sites that these species could diffuse into and simplify the conversion for FCC nickel to the NiO lattice structure.

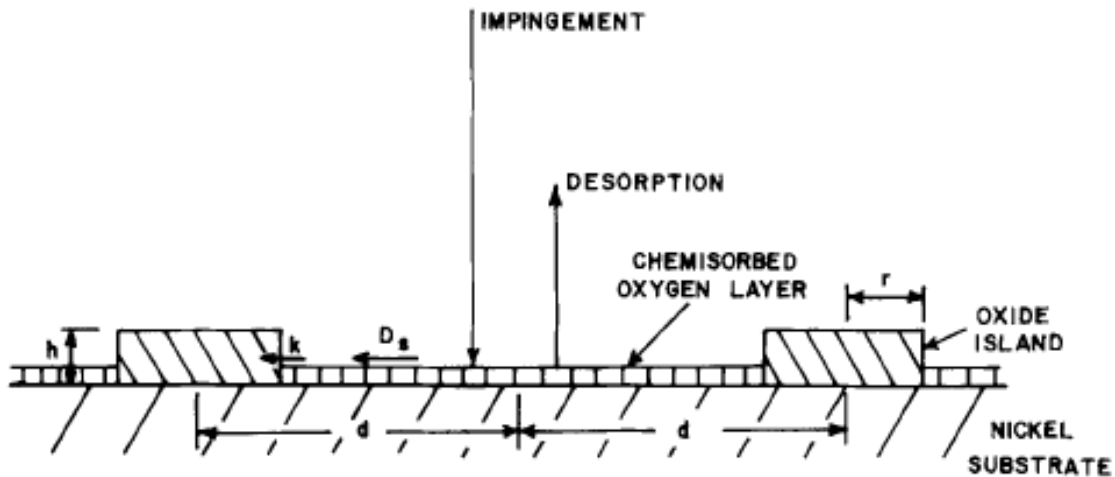


Figure 7: Schematic of accepted model of NiO formation via oxidation of pure nickel.^[36]

In the simulation, a two-dimensional hemispherical representation of the initial nickel particle was constructed. Nickel atoms were placed in the particle so as to form a FCC structure. Nickel atoms would have been removed to account for the equilibrium vacancy concentration, however the calculated vacancy concentration was too small to expect even one vacancy. The nickel atoms were allowed to move between lattice sites along closed packed directions and only via self-diffusion, but the boundary conditions and lack of vacancies prevented motion. Oxygen molecules adsorbed on the nickel surface were randomly assigned to the region immediately adjacent to the particle, which represents the particle surface. The number of oxygen molecules was arbitrarily set to 4 since a simulation error would occur if no oxygen molecules existed at the onset of the simulation, and calculations based on atmospheric oxygen density were unsatisfactory. The simulation allowed movement of the oxygen molecules along the surface of the nickel and into the bulk, as well as dissociation in atomic oxygen. The atomic oxygen was allowed motion via substitutional diffusion into vacant lattice sites and interstitial diffusion into vacant interstitial sites. The nickel and atomic oxygen could form NiO by bonding with neighboring atomic oxygen and nickel atoms, respectively. The bonded

nickel and bonded oxygen could continue to move via the same mechanisms allowed for the FCC nickel and atomic oxygen.

In keeping with the KMC approach, a single particle was randomly chosen from the simulation region during each time step to undergo a process, either diffusion or a chemical reaction. The probability of a given process occurring was weighted by the rate constant provided for that process, such that faster processes were more probable than slower ones and tended to be chosen more often. If the chosen particle could not undergo any processes, the simulation cycles through the remaining particles until one was chosen that successfully underwent a process. The configuration of particles in the simulation was updated, the simulation clock was incremented by the time step calculated as the reciprocal of the fastest rate constant, and the entire process was repeated.

Generally, the rate constant was composed of the product of a vibrational term and a Boltzmann factor, with the activation energy depending on the process. In the case of diffusion, the activation energy was based on the diffusing particle and medium. The rate constant also depended on whether a vacancy existed in the destination of a hop. If no vacancy existed, the rate constant for moving in that direction was set to zero. For chemical reactions, the activation energy was the activation energy of the particular reaction in the case of NiO formation or the enthalpy of the reaction in the case for the endothermic dissociation of O₂. The reaction rate constant was also weighted based on the presence of compatible reaction particles in close proximity of the chosen particle. If no such particles existed, the reaction probability was set to zero. For oxygen dissociation, the rate constant was weighted by the presence of a near-neighbor vacancy to place the second atomic oxygen atom released by the dissociation.

The motion of bonded nickel and bonded oxygen required additional considerations, as simply moving between two open sites required the chosen atom to break bonds and potentially form new ones. Given the exothermic nature of the NiO formation reaction, energy was released upon bond formation and must be provided for bond breaking. Thermodynamically, an increasingly exothermic reaction is more likely to occur when entropic effects are constant. This implied that the probability of a KMC process occurring that also involved a chemical reaction would be more likely for increasingly exothermic reactions. For diffusion of bonded nickel/bonded oxygen, the reaction was exothermic if more bonds were formed than were broken and was endothermic if fewer bonds were formed than were broken. Thus, motion along directions affording fewer bonds should be less favored, directions affording more bonds should be more favored, and directions affording no net change in number of bonds should be unchanged. In addition, oxygen bonding to nickel disrupted nickel-nickel bonds that exist between near neighbors in an FCC nickel lattice and required additional energy input. To include this behavior, interaction energies for the change in nickel-oxygen bonds and nickel-nickel bonds were added to the diffusion activation energy in the argument of the Boltzmann factor in the rate constant.

Given that some particles were unable to undergo any process due to surrounding particles or lack thereof, the program searched the simulation region for a particle that could undergo a process. To prevent repeated selections, any particle chosen was immediately removed from the particle reference list for random choosing in that time step before the chosen particle was evaluated for allowed processes. Once a suitable candidate particle was located, the available processes were determined and compiled

into a single list. A random process was chosen and then executed, with potential secondary processes also evaluated. For example, choosing a process that moved a bonded oxygen atom also reverted any bonded nickel that surrounded the oxygen to normal nickel if no other bonded oxygen were around those nickel atoms. At the same time, any nickel atoms surrounding the chosen destination of the moving bonded oxygen were changed to bonded nickel. If no nickel neighbors existed at the destination, the bonded oxygen atom was itself reverted to atomic oxygen. In this way, the chosen process required secondary actions to achieve greater realism.

In order to facilitate the process of designing an optimum nanoparticle, as well as the process of modeling characterized nanoparticles, several parameters can be varied. Changing the particle diameter and the contact angle with the $ZnWO_4$ particle will alter the geometry of the particle. Changing the vacancy concentration will alter the relative probability of different diffusion processes and may alter the oxidation behavior. Changing the number of initial oxygen molecules can enhance or reduce the overall rate of NiO formation. Changing the total time of oxidation can also greatly change the extent to which NiO forms and the composition of the particle at simulation conclusion.

Based on conversations with Professor Ray Phaneuf, motion of molecular oxygen in the air was removed so as to focus solely on the nickel oxidation. To that end, the simulation region was confined to a hemispherical region several elements wider and taller than the established nickel nanoparticle. Previous iterations began with molecular oxygen in air, but the current version begins with adsorbed molecular oxygen already on the nickel surface. In order to maintain a constant molecular oxygen concentration due to exposure to the atmosphere, replacement oxygen molecules were randomly generated in the simulation region following dissociation reactions. Due to the limited number of acceptable adsorption sites, a replacement oxygen molecule was not always generated. A secondary oxygen supply was included, based on the molecular oxygen impingement rate, the Boltzmann factor for forming a surface bond, and an term decreasing the replacement rate with current surface coverage.

Simulation Schematic:

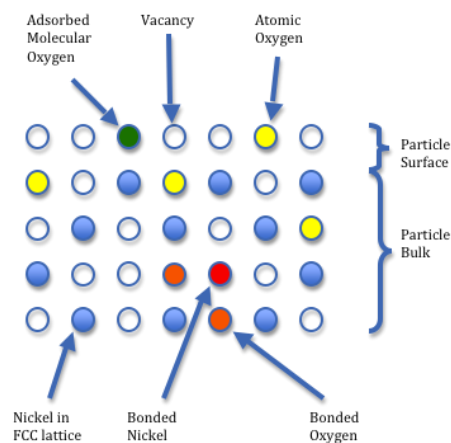


Figure 8: Schematic of the various particles or vacancies present in our NiOx sample. It is important to note that the concentrations of particles shown in the diagram are not representative of our system.

Species:

- 0 = vacancy
- 1 = nickel atom (in FCC lattice)
- 2 = molecular oxygen in air (**No Longer Used**)
- 3 = molecular oxygen adsorbed onto nickel surface
- 4 = atomic oxygen free
- 5 = atomic oxygen bonded to nickel atom (near neighbors)
- 6 = nickel atom bonded to oxygen atom (near neighbor)

Processes:

- 0. Vacancy = none

- 1. Nickel (FCC)
 - (a). Move diagonally along FCC lattice sites, [110] direction
 - (b). Bond to neighboring atomic oxygen (change FCC nickel to bonded nickel and change relevant atomic oxygen to bonded oxygen)
- 2. Molecular oxygen in air (**No Longer Used**)
 - (a). Move in air (up, down, left, right), [100] direction
 - (b). Move onto nickel surface and stick
- 3. Molecular oxygen adsorbed onto surface
 - (a). Move across nickel surface (up, down, left, right), [100] direction
 - (b). Dissociate into 2 atomic oxygen (if vacancy available)
- 4. Atomic oxygen
 - (a). Move (up, down, left, right), [100] direction
 - (b). Move diagonally between interstitial sites, [110] direction
 - (c). React with near-neighbor nickel atom (atomic nickel changed to bonded oxygen and relevant FCC nickel changed to bonded nickel)
- 5. Atomic oxygen bonded to near-neighbor nickel
 - (a). Move (up, down, left, right), [100] direction
 - i. Break bond and revert to free atomic oxygen (if no nickel near-neighbors at hop destination)
 - ii. Break and reform bonds (if nickel near-neighbors present at hop destination)
 - (b). Move diagonally between interstitial sites, [110] direction
- 6. Nickel (bonded to near-neighbor oxygen atoms)
 - (a). Move diagonally along FCC lattice sites, [110] direction
 - i. Break bond and revert to FCC nickel (if no bonded oxygen near-neighbors at hop destination)
 - ii. Break and reform bonds (if bonded oxygen near-neighbors present at hop destination)

Process Rates:

Temperature = 350 degrees C = 632.15 K

For atoms in solid, diffusion rate based on $k \sim 10^{13} \cdot \exp(-E_a/RT)$

Nickel Diffusion in FCC Nickel

$$E_a = 279.7 \text{ kJ / mol}^{[27]}$$

$$k \sim 9.17 * 10^{-11} \text{ Hz}$$

Oxygen Diffusion in FCC Nickel

$$E_a = 164 \text{ kJ / mol}^{[26]}$$

$$k \sim 0.310 \text{ Hz}$$

Nickel Diffusion in NiO

$$E_a = 36.6 \text{ kcal / mol} = 153 \text{ kJ / mol}^{[25]}$$

$$k \sim 4.26 * 10^{-1} \text{ Hz}$$

(does not consider effect of bond breaking, which is calculated each time step)

Oxygen Diffusion in NiO

$$E_a = 51.0 \text{ kcal / mol} = 213 \text{ kJ / mol}^{[25]}$$

$$k \sim 2.50 * 10^{-6} \text{ Hz}$$

(does not consider effect of bond breaking, which is calculated each time step)

Ni-O Interaction Energy

$$(1/2) \text{ O}_2 + \text{Ni} \rightarrow \text{NiO}: \Delta H^0 = -53.7 \text{ kcal/mol} = -239.74 \text{ kJ/mol}^{[23]}$$

$$\text{O}_2 \rightarrow 2 \text{ O}: \Delta H^0 = 498.37 \text{ kJ/mol}^{[24]}$$

$$\text{O} + \text{Ni} \rightarrow \text{NiO}: \Delta H^0 = (-239.74 - 0.5(498.37)) \text{ kJ/mol} = -488.92 \text{ kJ/mol}$$

Ni-O Interaction Energy $E_{\text{Ni-O}} = 488.92 \text{ kJ/mol}$ (for 298.15 K (25 °C))

Ni + O \rightarrow NiO Reaction Rate Constant

$$E_a = 76 \text{ kJ / mol}^{[35]}$$

collision cross-section: $\sigma = \pi * (\text{O radius} + \text{Ni radius})^2$

$$\text{O radius} = 0.60 \text{ angstroms}^{[32]}$$

$$\text{Ni radius} = 1.35 \text{ angstroms}^{[32]}$$

$$\sigma = 1.19 * 10^{-19} \text{ square meters}$$

reduced mass: $\mu = m_o * m_{\text{Ni}} / (m_o + m_{\text{Ni}}) = 2.087 * 10^{-26} \text{ kilograms}$

number density of colliding particle: $N = 9.171 * 10^{28} \text{ cubic meters}$

collision frequency^[40]: $Z = N * \sigma * (8kT / (\pi * \mu))^{0.5}$

$$Z = 1.126 * 10^{13} \text{ Hz}$$

$$k \sim Z * \exp(-E_a / RT) = 6.182 * 10^6 \text{ Hz}$$

(orientation based parameter was 1 for oxygen)^[40]

Ni-Ni Interaction Energy

$$L = 12 * (\text{interaction E})^{[27]}$$

$$L = 425.3 \text{ kJ/mol (for 0 K)}^{[33]}$$

$$\text{interaction E} = 35.4 \text{ kJ/mol}$$

Replacement Molecular Oxygen Insertion Time

Impingement Rate^[29]: $\Psi = 2.63 * 10^{20} * P / (MT)^{0.5}$ atoms per square cm per second

$$\Psi = 3.963 * 10^{23} \text{ atoms per square cm per second}$$

$$= 3.963 * 10^{27} \text{ atoms per square meter per second}$$

$$= 3.963 * 10^9 \text{ atoms per square nm per second}$$

Adsorb Rate^[28] = Psi * Surface Area * exp(-69 kJ/mol/(R*T))*exp(-4.3*(Fraction Surface Coverage))

(in Hz, calculated each time step)

Replacement Time = 1/(Adsorb Rate)

(seconds, calculated each time step)

O2 Dissociation Rate Constant

Ea = 234.3 kJ/mol^[31]

k~ 2.29 * 10⁽⁻⁷⁾ Hz

(for vibrational frequency of 10⁽¹³⁾ Hz)

O2 Diffusion Rate Constant

Ea = 523 kJ/mol^[31]

k~1.44*10⁽⁻³¹⁾ Hz

Assumptions:

- Entire simulation is 2-dimensional
- Nickel particle begins as single crystal of FCC nickel, with the (100) plane aligned with the lower boundary of the simulation zone
- Nickel particle has a constant diameter of 12 nm and a variable contact angle with respect to the lower boundary, which represents the ZnWO4 particle
- Lower boundary is flat rather than curved, since the error associated with excluding boundary curvature (based on nickel diameter and ZnWO₄ diameter) is roughly 0.5 unit cells at largest value
- ZnWO₄ does not interact with the oxygen or the nickel beyond acting as a substrate for the nickel (hence, not included in actual simulation region)
- Region around the particle represents the air, which is composed exclusively of molecular oxygen at 21% of air concentration
- The only inter-atomic interactions are between near-neighbors (up, down, left, right), longer range neighbors are also considered for motion of bonded oxygen and bonded particles
- Nickel atoms cannot move through or occupy interstitial sites in the FCC structure, and movement is only along [110] direction into lattice sites with vacancies (diagonally)
- Oxygen atoms/molecules can occupy lattice sites and interstitial sites, and can move along [100] direction into near-neighbor vacancies (up, down, left, right) or along [110] direction between interstitial sites
- Any molecular oxygen that adsorbs to the nickel surface does not desorb
- Atomic oxygen do not recombine to form molecular oxygen

- Defects such as edge and screw dislocations, twin boundaries, and stacking faults do not form
- Ignored the stress associated with the larger lattice parameter of NiO compared to FCC nickel
- Ignored possible stress from lattice mismatch between FCC nickel/NiO and the ZnWO₄ substrate
- Nickel particle surface represented by “smooth” hemisphere rather than FCC Wulff construction
- Given that atoms in nickel and NiO both exhibit FCC structure (NiO has two interpenetrating FCC lattices, one each for nickel and atomic oxygen), the lattice sites for the nickel atoms were fixed throughout the entire simulation to preserve a FCC structure

Fabrication

Of the two stages of fabrication, the synthesis of the ZnWO₄ and the deposition of NiO_x, both have been completed. For the first synthesis trial, 5 grams total of Zn(NO₃)₂ * 6H₂O and Na₂WO₄ * 2H₂O were mixed at 1:1 molar ratio in 90 mL distilled water. A white precipitate formed immediately and the mixture was sonicated for 30 minutes to ensure that most of the precursors reacted to form ZnWO₄. After sonication, the mixture was filtered for 3.5 hours, and washed with ethanol. The collection on the filter, a white paste, was then scraped off and dried at 84 °C for four hours. After drying the ZnWO₄ particles they were calcined at 500 °C for four hours in an alumina ceramic crucible. The end mass of the particles was significantly less than the mass of the precursors, with the majority of the loss resulting from the filtration step. A significant amount of particles passed through the filter, and not all of the particles were scraped off of the filter. While there was sufficient material for some characterization methods, such as XRD and particle size analyzer, more was needed for our testing and deposition of NiO_x. A second synthesis was conducted, starting with five times the precursor, 25 grams total of a 1:1 molar ratio of Zn(NO₃)₂ * 6H₂O and Na₂WO₄ * 2H₂O in 450 mL distilled water. The mixture was sonicated for 45 minutes because our XRD results showed that about 15.69% of the calcined particles were Na₂WO₄, and it is possible that a longer sonication will encourage more Na₂WO₄ particles to react. After sonication, the mixture was filtrated with multiple filters; the particles were washed with ethanol. The residue was collected from the filter paper and dried at 84 °C for nine hours. Then the powder was calcined at 500 °C for four hours. For the third batch of ZnWO₄ tungstate particles we used a 1:0.7 molar ratio of Zn(NO₃)₂ * 6H₂O and Na₂WO₄ * 2H₂O and made sure to crush the Na₂WO₄ to minimize the amount of Na₂WO₄ remaining after calcination.

The first batches of ZnWO₄ had Ni deposited simultaneously, following the exact same procedure. First the particles were added to 20 mL DI water, and then 1 wt% Ni(NO₃)₂ was added to each vial. The vials were stirred on a hotplate at 80 °C until dry. Then, the powders were calcined at 350 °C for an hour to oxidize the Ni that was just deposited onto the ZnWO₄ nanoparticles. At this point the particles were finished and ready for characterization and testing.

For the third batch of ZnWO₄ nanoparticles we used 2 wt% Ni(NO₃)₂ because we noticed very little Ni in the SEM, and the XRD results predicted 0.00% Ni. 40 mL of DI water was added and the mixture was dried on a hotplate at 80 °C like before. The

powder was calcined at 350 °C for an hour, and the batch was ready for testing.

Characterization

The main characterization tools in our project were X-Ray Diffraction (XRD), Scanning Electron Microscopy (SEM) and particle size analysis. We performed XRD analysis for three different samples, SEM analysis for five different samples and particle size analysis for 5 different samples. The XRD pattern of our first ZnWO₄ sample is shown in Figure 9 below:

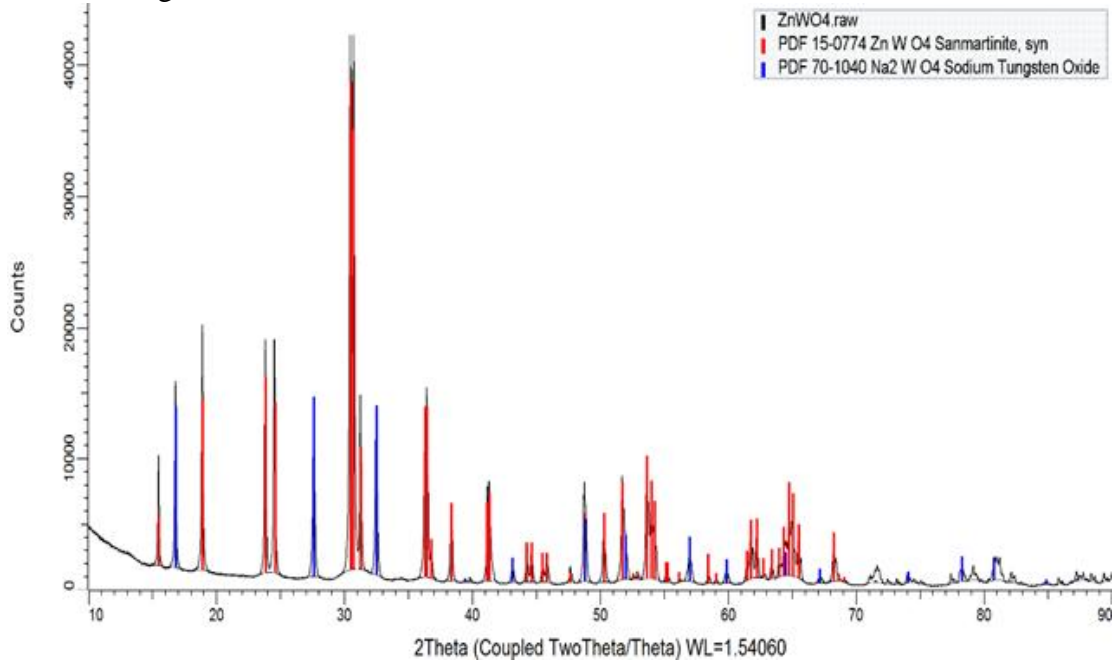


Figure 9: Shows the XRD schematic of our first ZnWO₄ sample. The black lines denote the observed spectrum, while the red and blue curves show the ZnWO₄ and Na₂WO₄ phases respectively.

The XRD distribution from our initial batch shows that two materials were present in our sample; ZnWO₄ and Na₂WO₄. Analysis of the pattern determined that there is approximately 84.310 wt% of ZnWO₄ and 15.690 wt% of Na₂WO₄. The Na₂WO₄ phase is undesired, but is hypothesized to come from an incomplete reaction between our two precursors. We were able to improve the composition of our final batch to 89% ZnWO₄ by decreasing the molar ratio of the Na₂WO₄ precursor and increasing the sonication time. In addition to determining the sample composition, XRD has also been useful for determining the average crystal size, the lattice parameters of our crystal, and other material properties. The properties for the first sample are shown in Table I below:

Table I: Provides the data output of the ZnWO₄ phase from the XRD experiment. The tables include ample useful information, but the main properties that our group is focusing on are the density, lattice parameters, crystal size, and wt%.

Structure 1							
Phase name				Structure			
R-Bragg				3.772			
Spacegroup				P12/c1			
Scale				0.00362624226			
Cell Mass				626.476			
Cell Volume (Å ³)				132.35415			
Wt% - Rietveld				84.310			
Crystallite Size							
Cry size Lorentzian (nm)				130.7			
Strain							
Strain L				0.02148987			
Crystal Linear Absorption Coeff. (1/cm)				892.177			
Crystal Density (g/cm ³)				7.860			
Lattice parameters							
a (Å)				4.6925262			
b (Å)				5.7220349			
c (Å)				4.9295340			
beta (°)				90.621			
Site	Np	x	y	z	Atom	Occ	Beg
Zn1	2	0.50000	0.68580	0.25000	Zn+2	1	0.56
W1	2	0.00000	0.18140	0.25000	W+6	1	0.4
O1	4	0.21590	0.89370	0.43860	O-2	1	0.35
O2	4	0.25770	0.37280	0.40070	O-2	1	0.48

From Table I we find that our lattice parameters and crystal density align nearly perfectly with reported results, which tells us that we have high quality monoclinic wolframite ZnWO₄. The reported density for ZnWO₄ is 7.87 g/cm³ while our result shows 7.86 g/cm³. Furthermore the reported lattice parameters differ from our results by no more than a thousandth of an angstrom. The differences in reported density and lattice parameters are negligible and show that our sample is similar to the literature values^[4,7,8]. This is encouraging because it shows that we are already producing the right crystal structure, and that our fabrication process is partially successful. The average ZnWO₄ crystal size was found to be 130.7 nm for the above sample, which is lower than our target particle size. Subsequent XRD showed variation in the crystal of different samples. We were able to produce larger crystals in subsequent procedures with our latest sample having a crystal size of 150 nm. Later XRD analyses also showed improvement in the composition of our samples with the latest fabrication yielding a 89% ZnWO₄ powder.

In addition to XRD diffraction, we performed particle size analysis to gain further understanding of the size distribution of our catalyst powders. The equipment used for our particle size analysis was the Zetasizer Nano machine in the 1135 KEB. In our analysis, we dispersed a small amount of our sample powders in distilled water and inserted the cuvette into the machine, which employed light absorption techniques to determine the particle size distribution. A representative output from the Zetasizer Nano

is included in Figure 10 below:

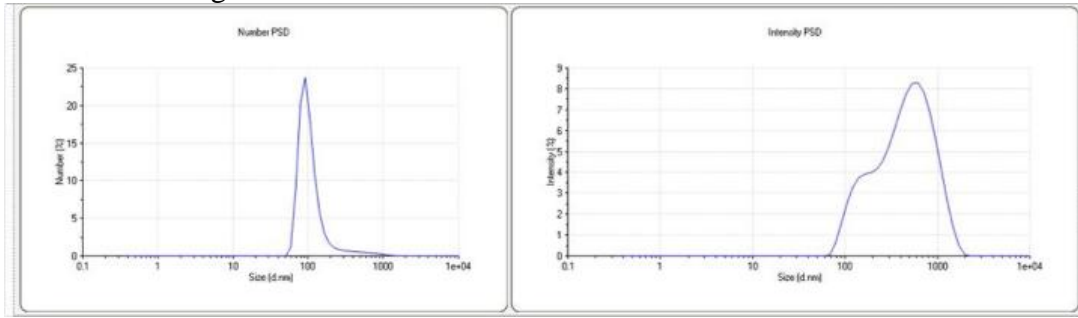


Figure 10: Particle Size Distribution (PSD) obtained from Zetasizer Nano; Number PSD (left) and Intensity PSD (right).

The output from the Zetasizer Nano includes graphs for the number and the intensity particle size distribution (PSD). The intensity PSD is the raw data from the equipment, yet this data is biased by the size of the particles, as large particles yield a higher intensity reading than small particle. The intensity PSD is transformed into the number PSD, which shows the actual distribution of particles in our samples. The number PSD for our sample in Figure 10 above is centered around 120 nm with a normal distribution. Overall, PSD from different samples showed an increase in particle size, indicating that the modifications we made to our fabrication yielded our desired effects. The data for additional PSD samples is included in the appendix.

The third characterization technique we used was Scanning Electron Microscopy (SEM). Given that our powders are not inherently conductive, we applied a small carbon coating to our sample in order to enhance the quality of our SEM output. We used the SEM pictures to determine how effective our fabrication process was in placing the NiOx particles on top of the ZnWO₄ substrate and also gained further insight into the uniformity of our particles. The SEM also allowed to gain further insight into the shape of our particles. A representative SEM picture is shown in Figure 11 below:

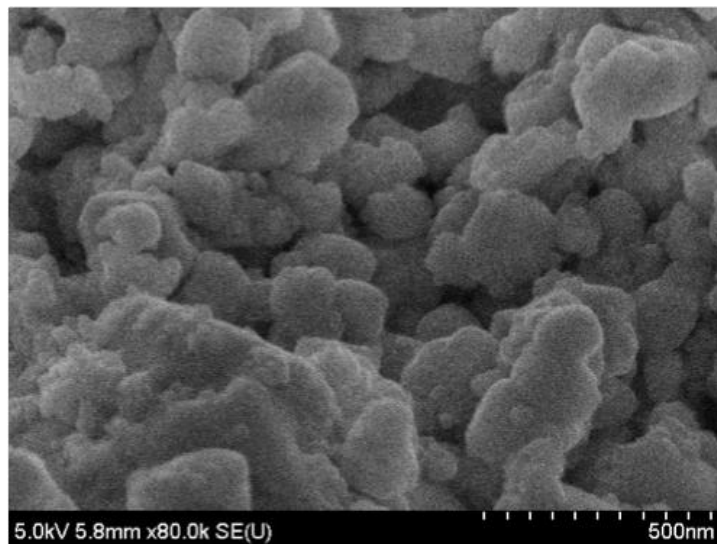


Figure 11: SEM output after NiOx deposition.

We also used the EDS capabilities of the SEM to determine whether all elements of interests were present in our samples. Our EDS analysis turned out inconclusive since the Zn peak and the Ni peak in the EDS spectrum are very close to each other, making it difficult to determine which peak in the EDS signal corresponds to the given element.

Results and Discussion

DFT Results

For ZnWO₄, the lowest energy configuration (seen in Figure 6) corresponded closely with the cell parameters measured experimentally. Since the NiO particles were not subjected to XRD measurements, the cell parameters for the materials are currently unknown and the lowest energy configuration for NiO cannot be compared to the experimental values. The values for c/a and a for the cells, both calculated and experimental can be found in Table I below.

Table II: The calculated and experimental cell parameters for ZnWO₄ and NiO.

Material	c/a (Calculated)	c/a (Experimental)	a (Calculated)	a (Experimental)
ZnWO ₄	1.223379	1.050508	4.744512	4.6925262
NiO	1.05	N/A	2.883756	N/A

In both cases, these plots and the configurations they indicate as ideal should be viewed as suspect due to a recent discovery concerning an error in the input files that were generated. Our group and the grad student who advised the Simulations team were unaware that for relatively small supercells like the two we were running, it is recommended to use a reciprocal-space projection scheme. The real space optimization is not efficient for small cells and it can also be less accurate for a calculation that is already known to result in inaccuracies for band gap calculations. The error is easily fixed and would be quickly addressed in any future work to be done for this project.

KMC Results

Simulations for a 0.0066 second (6.6 millisecond) oxidation of a 12 nm diameter nickel particle with contact angles of 30, 45, 60, and 90 degrees at a temperature of 350 degrees C were performed. Figure 12 shows how the fraction of oxidized nickel (bonded nickel/initial number of nickel) changed as a function of time and contact angle. To count as oxidized, a FCC nickel particle needed to react with at least one oxygen atom. The results show a trend of increasing oxidation with decreasing contact angle, likely due to the smaller contact angles with a constant particle diameter generating a nanoparticle with a lower volume of nickel that must be oxidized. Initially, all four sets of simulations showed increasing oxidation fraction with time. Contact angle of 90 degrees caused

oxidation to saturate at 0.077 within 0.0005 seconds (0.5 milliseconds), while a contact angle of 60 degrees caused oxidation to approach saturation at around the same time before continuing to increase and saturating at a fraction of 0.15 by 0.0028 seconds (2.8 milliseconds). This saturation may have resulted from the initially rapid dissociation of the constant molecular oxidation population creating a large number of atomic oxygen and by extension bonded oxygen. With the increase in the number of atoms that could undergo a process, the probability of choosing a molecular oxygen decreased to the point that new dissociation events became infrequent and the further atomic oxygen for bonding were rarely produced.

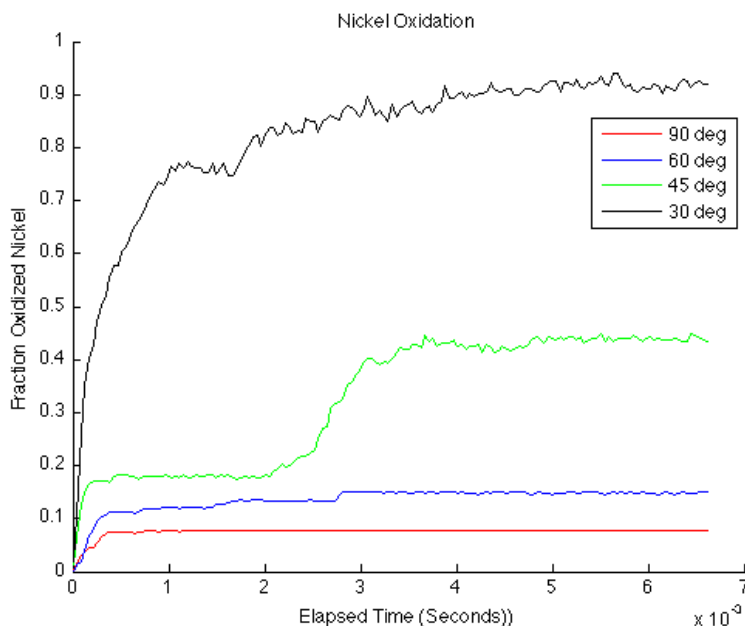


Figure 12: Fraction of oxidized nickel during KMC simulations of the 6.6 millisecond oxidation of 12 nm diameter nickel particle with contact angles of 30, 45, 60, and 90 degrees at a constant temperature of 350 degrees C. Time scale is in units of 10^{-3} seconds.

Contact angle of 30 degrees showed a continuing increase in oxidation fraction, though seems to stabilize around a fraction of 0.91. This may have resulted from the low number of nickel atoms present in the nanoparticle, so the initial rapid increase in atomic oxygen proceeded to oxidize a large fraction of the nickel particles. Also, the smaller system size meant the constant population of oxygen molecules represented a larger fraction of the whole population and thus dissociated more often. This led to a relatively large population of atomic oxygen during the entire course of the simulation, causing the continuous increase in oxidation fraction.

Contact angle of 45 degrees showed an initial saturation of 0.18 by 0.0005 seconds (0.5 milliseconds), but began increasing at 0.002 seconds (2 milliseconds) until saturating again at 0.43 by 0.0036 seconds (3.6 milliseconds). The cause may have been a large amount of nickel at the surface diffusing into the bulk after 0.002 seconds, or a sudden increase in the number of atomic oxygen available for bonding. To determine which

cause was behind the anomalous behavior, a plot of the fraction of bonded oxygen as compared to the maximum possible number of bonded oxygen is shown in Figure 13. The figure shows that the oxygen content increased at the same time as the increase in oxidized nickel for a contact angle of 45 degrees. This indicates that the oxidation increase was in fact caused by an increase in the amount of atomic oxygen and not a movement of oxygen from the surface to the bulk. The figure also supports the previous conclusions regarding the remaining three contact angles, since the saturation of oxygen for 60 and 90 degrees correlates to a quickly reduced dissociation probability, and the monotonic oxygen increase for 30 degrees correlates to a large dissociation probability that remained relatively constant throughout the simulation.

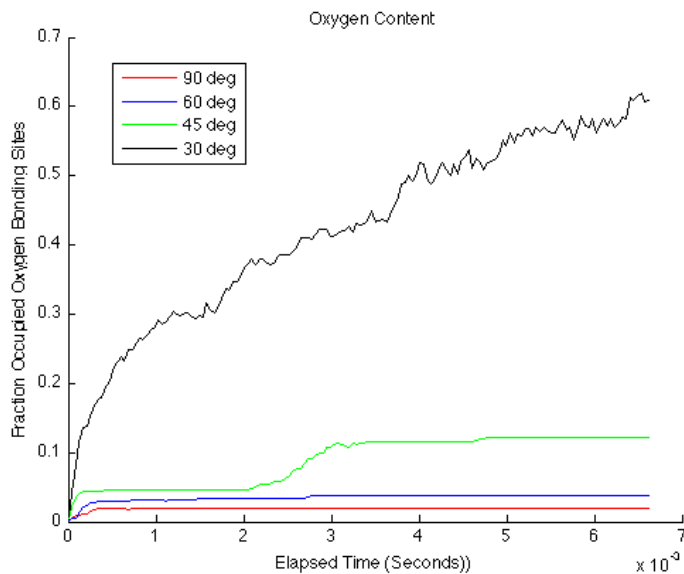


Figure 13: Fraction of fraction of bonded oxygen as compared to maximum possible number of bonded oxygen during KMC simulations of the 6.6 millisecond oxidation of 12 nm diameter nickel particle with contact angles of 30, 45, 60, and 90 degrees at a constant temperature of 350 degrees C. Time scale is in units of 10^{-3} seconds.

However, the cause of the increase in atomic oxygen during the simulation of the 45 degree contact angle still requires an explanation. To that end, Figure 14 shows a plot of the KMC simulation region at a time of 0.0026 seconds (2.6 milliseconds) for the 45 degree contact angle nanoparticle, close to the middle of the anomalous increase in nickel oxidation and oxygen content. The figure shows the presence four atomic oxygen atoms at the surface, as well as all four molecular oxygen residing close to each other on the left side of the particle. Based on the situation, a possible explanation arises in the form of the method of regenerating the oxygen molecules. When an oxygen molecule dissociated, a replacement was generated elsewhere in the region. If that replacement was generated near another particle, one of the directions of motion becomes zero and makes dissociation more probable. This could have caused a cascade effect that lead to an increase in the number of atomic oxygen, which would be amplified by the production of two atomic oxygen per dissociated molecule. With the impingement mechanism randomly adding a new molecular oxygen, this behavior becomes more likely. As such, the method of generating molecular oxygen in the system might be faulty, given that it included an instantaneous replacement and a impingement-based replacement. However,

a suitable method of quickly replacing the molecular oxygen is required since too few oxygen will limit oxidation and the literature showed that molecular oxygen was not in fact a rate limiting step in NiO formation^[38].

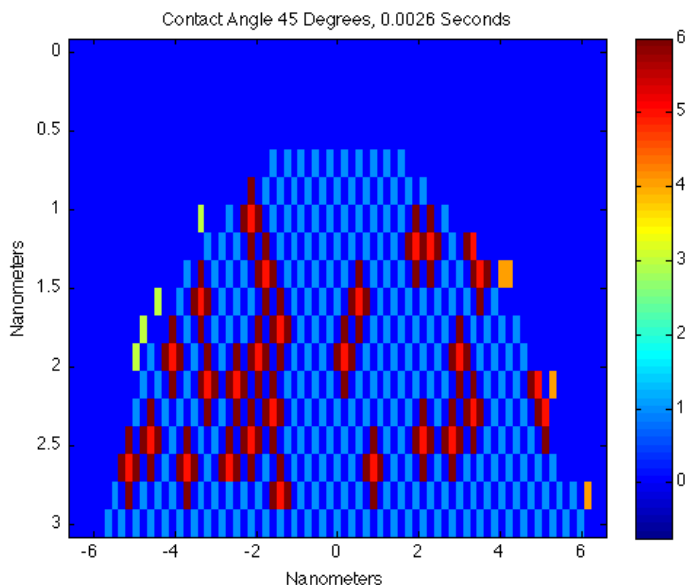


Figure 14: KMC simulation result for 2.6 millisecond oxidation of 12 nm diameter nickel particle with contact angles of 45 degrees at temperature of 350 degrees C.

Figure 14 also showed that the majority of the NiO at that time step existed within the nickel particle rather than at the surface. Examining the 30 degree contact angle particle at 0.0066 seconds in Figure 15 showed a similar distribution when considering that the bonded oxygen was expected to be more prevalent near surface than deep in the bulk. In fact, examining the simulation at various time steps for all contact angles revealed that the atomic oxygen rapidly bonded to the surface nickel and then diffused into the bulk, despite the extra energy barriers associated with disrupting the larger numbers of nickel-nickel bonds. As such, no constant surface layer of NiO formed during any of the runs and the simulation failed to emulate the expected oxidation behavior based in experiments from the literature.^[36] This likely explained the rapid degree of nickel oxidation, since the oxygen atoms were able to diffuse rapidly within the nanoparticle and bond to large numbers of nickel atoms. There may exist additional processes or effects that realistically reduce oxygen diffusion into the nickel bulk but which were not accounted for in the simulation. One such possibility is the stress induced by the oxygen increasing the lattice parameter from FCC nickel to 4.177 angstroms for NiO, which would present an additional energy barrier to oxygen diffusion in the nickel^[39]. Another is stress induced by lattice mismatch with the underlying ZnWO₄, which was treated as independent of the nickel oxidation except for providing a location for the nanoparticle to form.

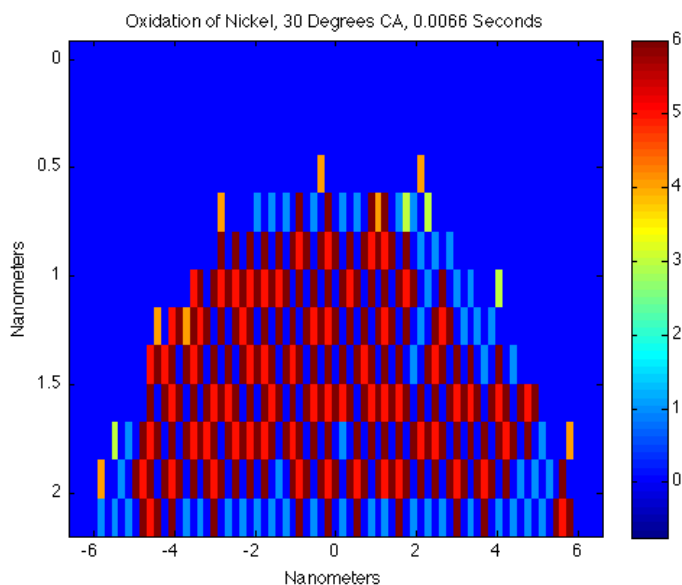


Figure 15: KMC simulation result for 6.6 millisecond oxidation of 12 nm diameter nickel particle with contact angles of 30 degrees at temperature of 350 degrees C.

Fabrication Results:

Many achievements were made with regard to our fabrication process. The samples prepared had very high crystallinity, often times being single crystals, and had a relatively good composition. While even the best samples still had some Na_2WO_4 the quantity was pretty minute compared to the amount of ZnWO_4 present. The team also deposited Ni on the ZnWO_4 substrate, and was able to oxidize the nickel. Based on our SEM photos, NiO particles of about 20-40 nm were present on many of the ZnWO_4 particles. However, the group was unable to definitively confirm whether these particles were definitively NiO, due to time constraints and the limitations of XRD and SEM. The design called for particles in the 400 to 500 nm range, but the samples appeared to be slightly smaller. Most of the particles produced were around 100- 130 nm. The fabrication procedure actually used during prototyping was nearly exactly as predicted during our design stage, which demonstrates that amount of thought that went into our original design procedure.

Characterization Results:

As previously mentioned, the main characterization techniques employed were XRD, SEM, and particle size analysis. Our final XRD analysis showed that our samples consisted of 89% ZnWO_4 and 11 percent Na_2WO_4 with trace amounts of Ni. This final composition is an improvement from our initial batch, but we intend to continue optimizing our fabrication in the future. Together the XRD and the particle size distribution allowed us to determine that our particles had very high crystallinity, and were smaller than desired. On some occasions, the crystal size given by our XRD

analysis would exceed the center of the PSD given from the Zetasizer Nano. We attribute this discrepancy to the fact that our particles may be too large to apply to Scherrer formula, which was used to determine our crystal size. Application of the Scherrer formula for our particles would yield a crystal size that is larger than the actual crystal, which corresponds to the measurements we observed. SEM informed us on the relative uniformity of our samples which is a good indicator. At the same time, SEM also showed some agglomeration which told us that there might not be sufficient dispersion of our particles. An SEM picture of our sample is shown in the figure below.

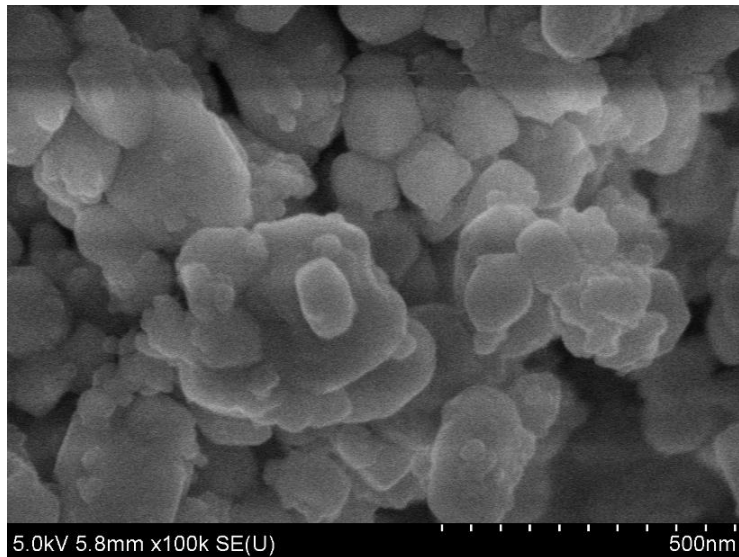


Figure 16: This SEM picture shows the relative size and shape of our ZnWO_4 nanoparticles. The smallest particles, around 20-40 nm, are hypothesized to be our NiO particles.

Figure 16 is an SEM picture which shows the relative size and shape of our ZnWO_4 nanoparticles. The figure also shows smaller particles which we believe are our NiO particles. We have come to this conclusion because those smaller particles were not present prior to our NiO deposition process. This picture demonstrates that the average ZnWO_4 particles are roughly around 100-200 nm but that there are some significantly larger particles. We believe that some of these larger particles are due to agglomeration and others are just larger crystals. This particles in this picture are fairly uniform for all of your samples, and provides an accurate representation of what our fabrication process produced.

These characterization methods allowed our group to determine the sample's properties and provided us with the necessary information to consistently update our fabrication procedure throughout the semester. Due to time and monetary constraints, we were not able of using BET to measure the surface area of our particles. This was determined to be a second hand factor to the particles performance and to our design, so we left it for future work.

Performance testing was done using the Solar Simulator located in the FabLab. As a result of not having access to a gas chromatograph and not seeing any bubbles produced after illumination, our performance is inconclusive. We did notice that some condensation was formed on the side of our container, but we are unsure whether that is from hydrogen production or the vapor pressure of water. It is important to note

that the high intensity light did increase the temperature of our particle suspension up to 35 C. While this is still relatively low compared to the boiling point of water, there is still increased amounts of water vapor produced at this temperature. For any conclusive performance results to be made additional testing is required and a more accurate method of measuring hydrogen production is necessary.

Updated Schedule

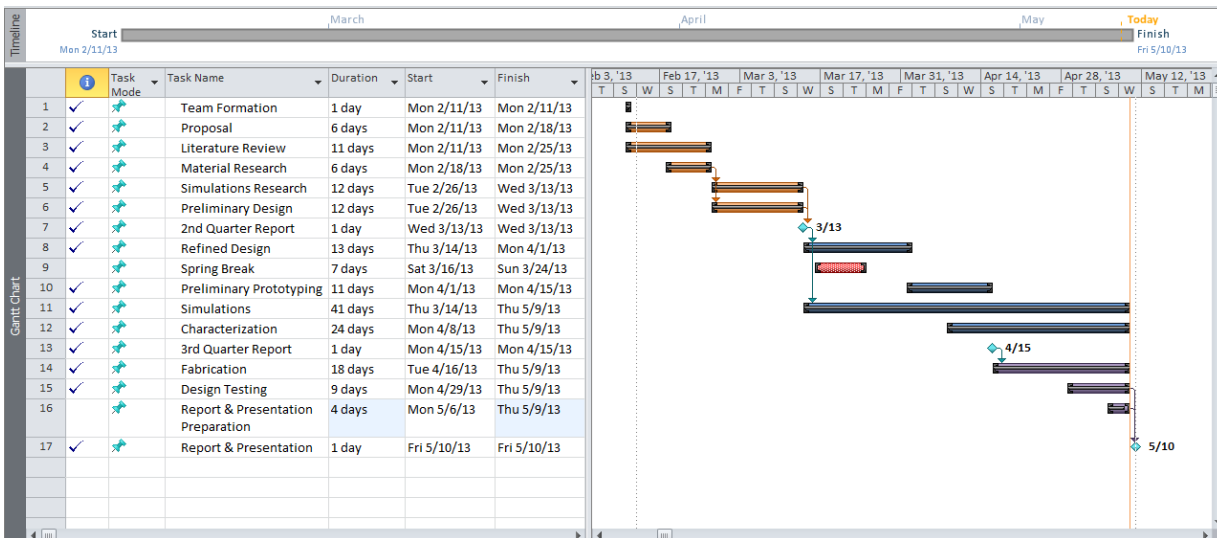


Figure 17: Project Schedule.

Team Member Roles and Responsibilities

- The Executive Committee is responsible for administrative duties and managing the overall project.
- The Communications Lead is responsible for managing communications within the team.
- The Simulations Committee Lead is both the technical and administrative lead on the simulation component of the project. This role has been split into two sub-positions, DFT Lead and Kinetics Lead, which will coordinate to ensure the efficient running of the Simulations Committee.
- The Research Committee Lead is both the technical and administrative lead on the research component of the project.
- The Fabrication Committee Lead is both the technical and administrative lead on the fabrication component of the project.
- With the exception of the Executive Committee, no committee positions except for the committee lead will be assigned to a given committee. This will promote flexibility among team members to contribute to the project according to their strengths and interests and will allow the team to cater work towards project needs.

Table III: Assigned Roles for Each Group Member

Committee	Position	Team Member
Executive	Project Leader & Sponsor Point of Contact	Nicholas Faenza
Executive	Secretary	Mark Reese
Executive	Treasurer & Editor	Norena Beaty
Communications (Internal)	Communications Lead	Owen McGovern
Simulations	KMC Lead	Tanner Hamann
Simulations	DFT Lead	Norena Beaty
Research	Research Lead	Santiago Miret
Fabrication	Fabrication Lead	Owen McGovern

Conclusions

The photocatalytic system studied, designed and fabricated involved the use of ZnWO_4 as the main photocatalyst with smaller NiO co-catalysts adhered to the surface. The designed system was based off of factors such as the electronic band structure, the kinetic rates of oxidation, and various material properties. The resulting design was fabricated, characterized and tested for performance. The project met nearly all of its design goals, and if additional time was provided each goal would have been surpassed.

The first goal was to use DFT to calculate the electronic structure of our two photocatalysts. The electronic structure entailed both the band gap of the materials and the band edge placements with respect to the energy levels of redox reactions. Our team wanted to calculate this data as well as see how it varied as a result of change adsorption angle of NiO on ZnWO_4 . While specific band diagrams were not created as anticipated, the first round of energy relaxations were successfully run and analyzed. Unfortunately, the first round of relaxations would have to be rerun due to the calculations being done in real-space coordinates instead of reciprocal-space, which increased the likelihood of inaccuracies in the results. Only a second set of relaxations and a final bulk calculation, as well as an analysis of those results would remain if these relaxations were run again. If given more time, the group would complete the DFT calculations that give band structures as a function of adsorption angle of NiO, compare the results to the measured

values for NiO, and use those results to recommend a synthesis procedure that results in a nanoparticle structure that optimizes the band gap of the system for maximum UV absorption.

Another team goal of ours was to use a kinetic Monte Carlo simulation to understand the kinetics behind oxygen absorption and diffusion through our nickel particles. Similar to DFT, our simulation was nearly complete but still required a few touch ups. Currently, we have completed 0.0066 second-long simulations for 12 nanometer-diameter nickel particles with four contact angles. The results show that the rate of overall oxidation increases with decreasing contact angle due to the lower particle volume. However, simulation emphasized diffusion of atomic oxygen into the nickel bulk over diffusion along the surface, leading to most of the NiO residing within the particle and little NiO at the surface. Based on literature, the initial stage of nickel oxidation should show NiO islands nucleating and coalescing at the nickel surface to form a continuous oxide layer. Therefore, our simulation deviates from a key aspect of NiO formation, possibly due to the absence of additional physical processes or effects. One possibility is stress associated with oxygen atoms disrupting the nickel FCC lattice and expanding the lattice parameter during the transition from nickel to NiO. This would represent an additional energy barrier to oxygen diffusing into nickel and may bring the simulation more in line with observations. Our future work involves improving the O₂ generation process, allowing for movement of the nickel atoms, factoring in stress induced by the lattice parameter expanding from FCC nickel to NiO, and then running the simulation over a longer time scale. After these improvements are made our simulation will be complete and we can gain more accurate results regarding the necessary calcining time and temperature.

The design was successful in fully optimizing the material parameters based off of an in-depth research of the literature. The size, shape, crystal structure, crystallinity, and surface area were all important factors that went into determining our fabrication procedure and optimizing our design. Lastly, our group aimed to test our particles performance and then compare it to similar studies. Our results from testing proved to be inconclusive due to constraints over experimental setups. If given more time and resources, a proper performance test would be conducted which would allow our team to compare our photocatalytic system to others.

In conclusion, this project reached the majority of its goals, and if given more time would have accomplished everything that it aimed to. The team achieved successes in our DFT modeling, kMC simulations, and the fabrication of the sample. While our testing procedure provided inconclusive results, the team thoroughly analyzed the literature and used our knowledge in materials science and engineering to create a strong design for our photocatalytic system.

Future Work

At present, no vacancies are generated in the initial nickel lattice. This is based on the nickel vacancy formation energy of $1.4 \text{ eV} = 134.8 \text{ kJ/mol}$, the fraction of lattice sites that have vacancies is 4.92×10^{-12} , and the nickel nanoparticle contains at most several hundred lattice sites.^[34] As such, both FCC nickel and bonded nickel in this

current version of the simulation are unable to move. However, several studies concluded that nickel in NiO represents the primary diffusing particle, which appears to be substantiated by the resulting rate constants calculated for bonded nickel and bonded oxygen. Given the apparent failure of the simulation in regards to nickel diffusion in NiO, further research is required.

The work performed until this point using VASP is just the beginning of a thorough understanding of the electronic behavior of the ZnWO₄-NiO system. At present, all calculations beyond relaxations of the unit cells cannot be considered accurate, and there are some immediately apparent and feasible steps towards improving the reliability of our results. The first issue with our calculations is that they were performed using a real space projection scheme rather than a reciprocal space scheme; it was not discovered until all 100 relaxation calculations were complete that the real space projection was not appropriate for our situation and would result in inaccurate lattice parameters. Rectifying inaccuracies as a result of this is as simple as changing one line in the INCAR files and adjusting the primitive lattice vectors to reflect their reciprocal nature. This should bring our relaxed parameters closer in line with those experimentally determined via XRD. Band edge placement calculations would naturally follow to demonstrate the two catalysts as appropriate material choices for a z-scheme system. The final step is moving from bulk calculations to simulating the interface between the nickel oxide and zinc tungstate particles. Looking at the surfaces would allow us to make adjustments to our fabrication process based on optimized contact angles and co-catalyst particle size.

There is still a significant amount of fabrication and characterization work to be done in this project. Our fabrication procedure needs to be revised so that our samples are exactly what we designed for. For example our particle sizes were much smaller than the 500 nm that was designed. Our team would like to try calcining the ZnWO₄ for longer periods of time to allow for more crystal growth. In addition, further testing is required to understand why our average crystal size was found to be larger than our average particle size. More work is also needed concerning the NiO fabrication and characterization. Testing needs to be done to ensure that the 20-40 nm particles that we created are NiO as hypothesized. The amount of the NiO present in the final solution also needs to be calculated to see how much of the material is lost during the fabrication process. Our samples were never characterized with BET or any other method to determine the surface area. If we were given more time and resources we would make sure to do studies on how our fabrication procedure impacts the particles surface area and how we could experimentally optimize that.

Once our samples correlate with our design, we would like to continue the performance testing. For any future performance testing we realize that it is necessary to have a gas chromatograph to accurately measure the hydrogen production. Furthermore, better results may be achieved by using a high intensity UV lamp, instead of a solar simulator. Clearly, there is ample future work for not only fabrication and characterization but for nearly every aspect of this project.

Acknowledgements

Team H2 would like to acknowledge the following faculty and students for their generous support:

- Prof. Ray Phaneuf (Kinetics, Logistics)
- Prof. Oded Rabin (Fabrication)
- Prof. Eric Wachsman (Fabrication)
- Mr. Colin Gore (Fabrication)
- Prof. Isabel Lloyd (Characterization)
- Dr. Kai Zhong (Characterization)
- Dr. Robert Bonenberger (Characterization)
- Ms. Jane Cornett (Characterization)
- Mr. John Abrahams (Characterization)
- Prof. Ted Einstein (Simulation)
- Mr. Josue Morales (Simulation)
- Prof. Yifei Mo (Simulation)
- Maryland Nanocenter
- This work used the Extreme Science and Engineering Discovery Environment (XSEDE), which is supported by National Science Foundation grant number OCI-1053575.
- Department of Materials Science and Engineering

References

- [1] A. Kudo, Y. Miseki, "Heterogeneous photocatalyst materials for water splitting," *Chem. Soc. Rev.*, 2009, **38**, 253-278. DOI: 10.1039/B800489G
- [2] K. Maeda, K. Domen, "Photocatalytic Water Splitting: Recent Progress and Future Challenges," *The Journal of Physical Chemistry Letter*, 2010, 2655-2661. DOI: 10.1021/jz1007966
- [3] H. Kadowaki, N. Saito, H. Nishiyama, H. Kobayashi, Y. Shimodaira, Y. Inoue, "Overall Splitting of Water by RuO₂-Loaded PbWO₄ Photocatalyst with d10s²-d0 Configuration," *J. Phys. Chem. C*, 2007, **111**, 439-444. DOI: 10.1021/jp06656555m
- [4] H. Fu, C. Pan, L. Zhang, Y. Zhu, "Synthesis, characterization and photocatalytic properties of nanosized Bi₂WO₆, PbWO₄ and ZnWO₄ catalysts," *Materials Research Bulletin*, 2007, **42**, 696-706. DOI: 10.1016/j.materresbul.2006.07.017
- [5] W. Kohn, A. D. Becke, R. G. Parr, "Density Functional Theory of Electronic Structure," *J. Phys. Chem.*, 1996, **100**, 12974-12980. DOI: 10.1021/jp960669l
- [6] C. Hu, H. Teng, "Structural features of p-type semiconducting NiO as a co-catalyst for photocatalytic water splitting," *Journal of Catalysis*, 2010, **272**. DOI: 10.1016/j.jcat.2010.03.020
- [7] W. Yan, S. Zhang, L. Zhang, Y. Zhu, "Photocatalytic Activity of Nanosized ZnWO₄ Prepared by the Sol-gel Method," *Chem. Res. Chinese*, 2007, **23**, 465-468.
- [8] G. Huang, Y. Zhu, "Synthesis and photocatalytic performance of ZnWO₄ catalyst," *Materials Science and Engineering: B*, 2007, **139**, 201-208. DOI: 10.1016/j.mseb.2007.002.009
- [9] Y. Sasaki, A. Iwase, H. Kato, A. Kudo, "The effect of co-catalyst for Z-scheme photocatalysis systems with an Fe³⁺/Fe²⁺ electron mediator on overall water splitting under visible light irradiation," *Journal of Catalysis*, 2008, **259**, 133-137. DOI: 10.1016/j.jcat.2008.07.017
- [10] "University of Maryland MSE Seminar Series: Innovating Materials at the Nanoscale for Artificial Photosynthesis," Dunwei Wang, 2013.
- [11] "University of Maryland Course: Materials For Energy 1," Eric D. Wachsman, 2012.
- [12] D. Kanan and E. Carter. "Band Gap Engineering of MnO via ZnO Alloying: A Potential New Visible-Light Photocatalyst." *J. Phys. Chem*, 2012 C, **116**, 9876-9887. DOI: 10.1021/jp300590d

- [13] R. Jindal, M. Sinha, and H. Gupta, "Study of zone centre phonons in wolframite ZnWO_4 ," *Tubitak*, <http://online.journals.tubitak.gov.tr/openAcceptedDocument.htm?fileID=216961&no=40707>
- [14] Hilger Crystals Ltd., "Properties of ZnWO_4 ," http://www.hilger-crystals.co.uk/prior/mat_znwo4.htm
- [15] Segelstein, David J. *The complete refractive index of water*. MS Thesis. University of Missouri, Kansas City, 1981.
- [16] L. Mingyi, Y. Bo, X. Jingming, C. Jing. "Thermodynamic analysis of the efficiency of high-temperature steam electrolysis system for hydrogen production." *Journal of Power Sources*, 2008, **117**, 493–499. DOI: 10.1016/j.jpowsour.2007.11.019
- [17] "University of Maryland Course: Materials For Energy 2," Liangbing Hu, 2013.
- [18] S. Garruchet, O. Politano, P. Arnoux, V. Vignal. "Diffusion of oxygen in nickel: A variable charge molecular dynamics study." *Solid State Communications*, 2010, **150**, 439-442. DOI: 10.1016/j.ssc.2009.12.012.
- [19] A. Mills, S. Le Hunte. "An overview of semiconductor photocatalysis." *Journal of Photochemistry and Photobiology A: Chemistry*, 1997, **108**, 1-35. DOI: 10.1016/S1010-6030(97)00118-4.
- [20] T. Sreethawong, Y. Suzuki, S. Yoshikawa. "Photocatalytic evolution of hydrogen over mesoporous supported NiO photocatalyst prepared by single-step sol-gel process with surfactant template." *International Journal of Hydrogen Energy*, 2005, **30**, 1053-1062. DOI: 10.1016/j.ijhydene.2004.09.007.
- [21] Y. Wu, M. Chan, G. Ceder. "Prediction of semiconductor band edge positions in aqueous environments from first principles." *Physical Review B*, 2011, **83**, 1-7. DOI: 10.1103/PhysRevB.83.235301.
- [22] Mycyk, M.; Hryhorczuk, D.; Amitai, Y. "Lead." *Pediatric Toxicology: Diagnosis and Management of the Poisoned Child*, 2005. ISBN 0-07-141736-2.
- [23] B.J. Boyle, E.G. King, K.C. Conway. "Heats of Formation of Nickel and Cobalt Oxides (NiO and CoO) of Combustion Calorimetry." *Journal of the American Chemical Society* 76.14 (1954): 3835-837. Web. DOI: 10.1021/ja01643a072
- [24] B. deB Darwent. *Bond Dissociation Energies in Simple Molecules*. Rep. Washington, D.C.: National Bureau of Standards, 1970. Print. National Standard Reference Data Ser. Web. <<http://www.nist.gov/data/nsrds/NSRDS-NBS31.pdf>>

- [25] M. O'Keefe, W.J. Moore. "Diffusion of Oxygen In Single Crystals of Nickel Oxide." *The Journal of Physical Chemistry* 65.8 (1961): 1438-439. Web. DOI: 10.1021/j100826a039
- [26] J. Park, C.J. Altstetter. "The Diffusion and Solubility of Oxygen in Solid Nickel." *Metallurgical Transactions A* 18.1 (1987): 43-50. Web. DOI: 10.1007/BF02646220
- [27] D.A. Porter, K.E. Easterling, M.Y. Sherif. *Phase Transformations in Metals and Alloys*. 3rd ed. New York: CRC, 2009. Print.
- [28] B. Monnera, L. Kiwi-Minsker, A. Renken. "Mathematical Modelling of the Unsteady-state Oxidation of Nickel Gauze Catalysts." *Chemical Engineering Science* 58 (2003): 4911-919. Web. DOI: 10.1016/j.ces.2002.11.006
- [29] G.S. May, "Metallization." Lecture. ECE/ChE 4752: Microelectronics Processing Laboratory. Georgia Tech College of Engineering, Atlanta. 26 Feb. 2004. Web. 8 May 2013. <www.ece.gatech.edu/research/labs/vc/lectures/Lecture7.ppt>.
- [30] P.H. Holloway, J.B. Hudson. "Kinetics of the Reaction of Oxygen with Clean Nickel Single Crystal Surfaces: I. Ni(100) Surface." *Surface Science* 43.1 (1974): 123-40. Web. DOI: 10.1016/0039-6028(74)90223-4
- [31] Panas, I., P. Siegbahn, and U. Wahlgren. "The Mechanism for the O₂ Dissociation on Ni(100)." *Journal of Chemical Physics* 90.11 (1989): 6791-801. Web. DOI: 10.1063/1.456298
- [32] J.C. Slater. "Atomic Radii in Crystals." *J. Chem. Phys.* 41.10 (1964): 3199-204. Web. DOI: 10.1063/1.1725697
- [33] A.I. Zaitsev, N.E. Zaitseva. "Pressure of the Saturated Vapor of Nickel at High Temperatures." *High Temperature* 40.2 (2002): 197-202. Web. DOI: 10.1023/A:1015242921061
- [34] R.A. Johnson. "Point-Defect Calculations for an FCC Lattice." *Physical Review* 145.2 (1966): 423-34. Web. DOI: 10.1103/PhysRev.145.423
- [35] S.A. Raspopov, A.G. Gusakov, A.G. Voropayev, A.A. Vecher, and V.K. Grishin. "Enhanced Oxidation of Nickel in Atomic Oxygen." *Journal of Alloys and Compounds* 227.1 (1995): 5-9. Web. DOI: 10.1016/0925-8388(95)01643-0
- [36] P.H. Holloway. "Chemisorption and Oxide Formation on Metals: Oxygen–nickel Reaction." *J. Vac. Sci.* 18 (1981): 1964-982. Web. DOI: 10.1116/1.570847

[37] P.H. Holloway, and R.A. Outlaw. "The Effects of Temperature upon NiO Formation and Oxygen Removal on Ni(110)." *Surface Science* 111.2 (1981): 300-16. Web. DOI: 10.1016/0039-6028(80)90710-4

[38] J.A. Slezak, B.D. Zion, and S.J. Sibener. "Enhanced Oxidation Rate of Ni(111) by Atomic Oxygen." *Surface Science Letters* 442.1 (1999): L983-988. Web. DOI: 10.1016/S0039-6028(99)00941-3

[39] T. Bredow, A.R. Gerson. "Effect of Exchange and Correlation on Bulk Properties of MgO, NiO, and CoO." *Physical Review B* 61.8 (2000): 5195-201. Web. DOI: 10.1103/PhysRevB.61.5194

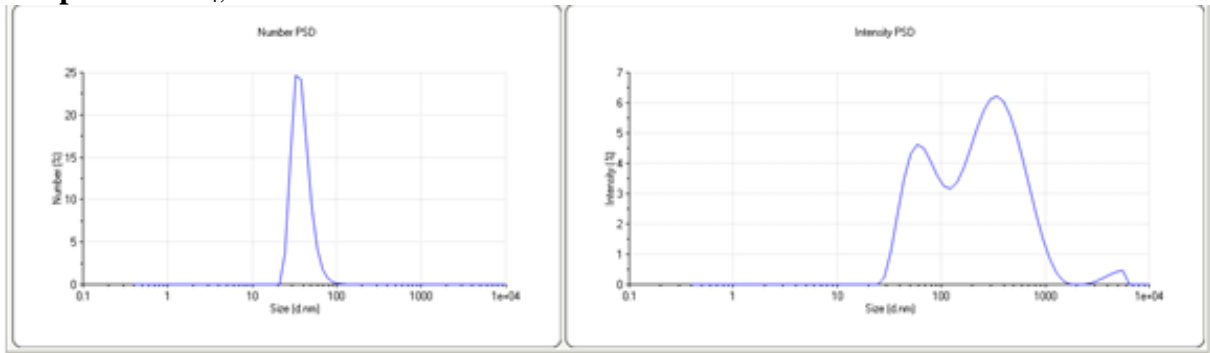
[40] Email. From R. Phaneuf. "RE: ENMA 490 Self/Peer/Group Evaluation." Email to T. Hamann. Received 7 May 2013.

Appendix

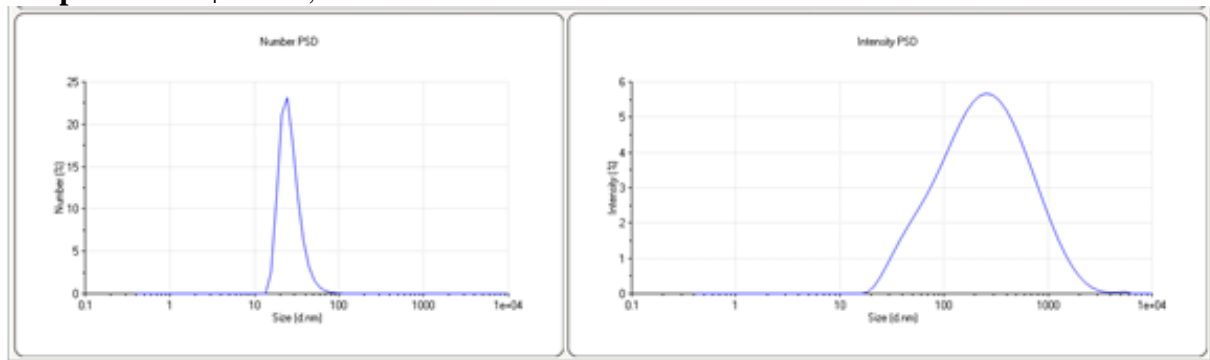
Zetasizer Nano Data:

The following diagrams are data taken from the particle size analyzer. Our sample names are arranged based off of the batch number that they were a part of and whether it is pure ZnWO_4 or both ZnWO_4 and NiO . There were a total of three batches produced, where batch 3 was the most recent. It is important to note that some samples have a particle size distribution while others only have an intensity distribution.

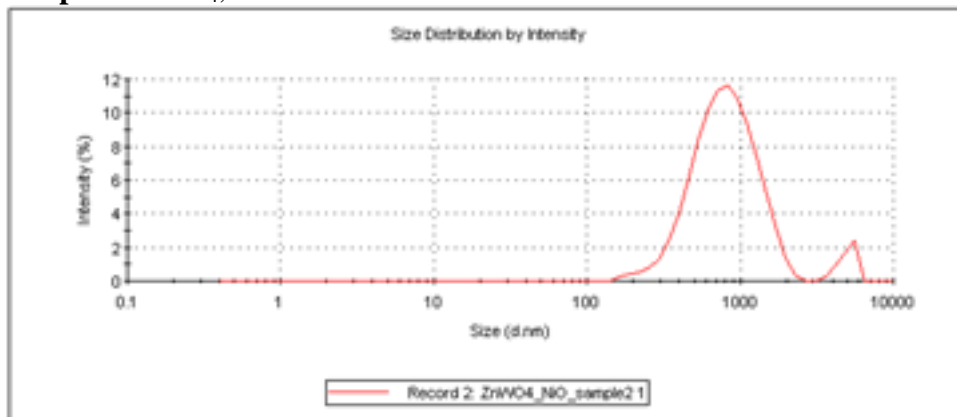
Sample: ZnWO_4 , batch #1



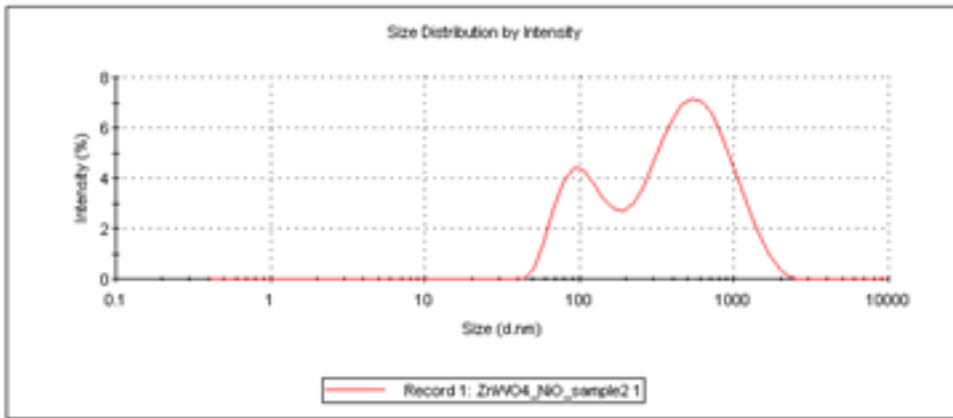
Sample: $\text{ZnWO}_4 + \text{NiO}$, batch #1



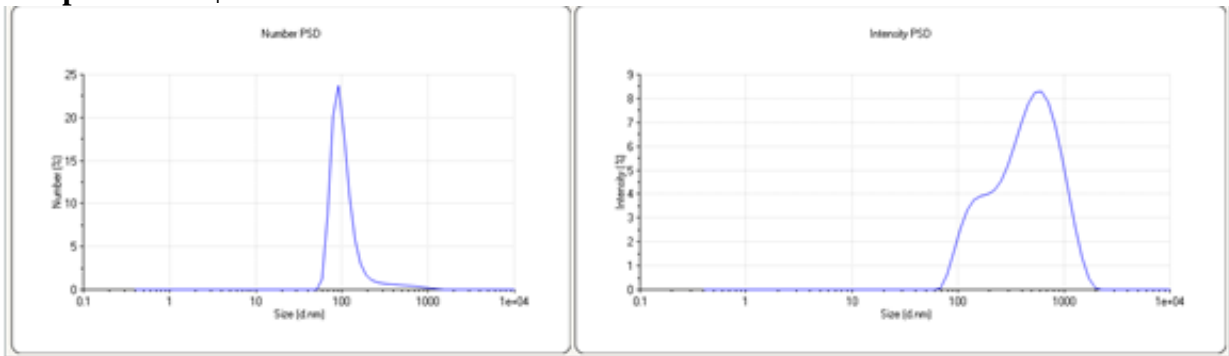
Sample: ZnWO_4 , batch #2



Sample: ZnWO₄ + NiO, batch #2



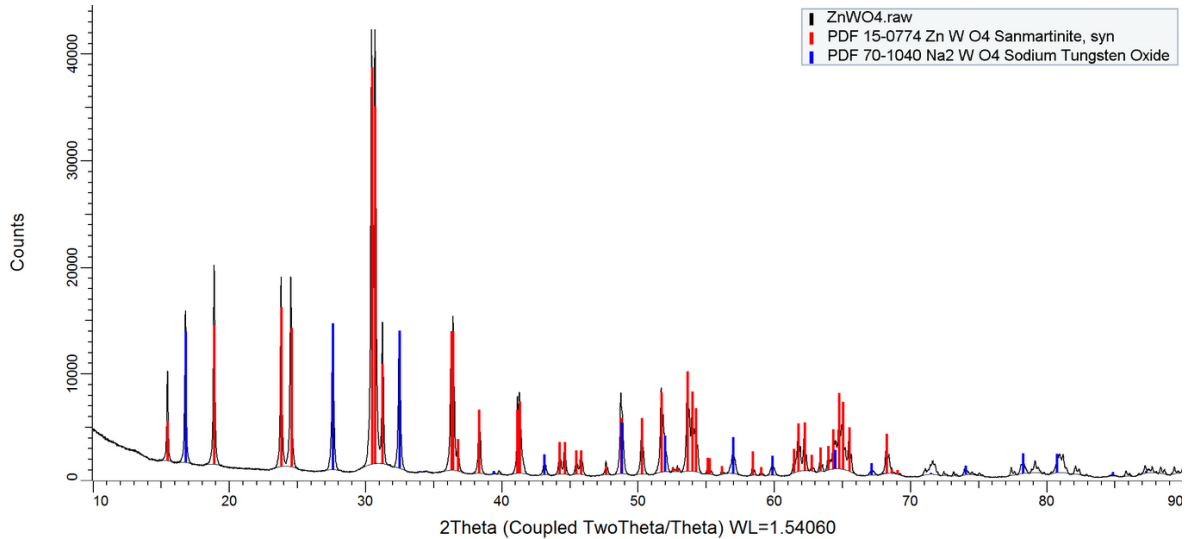
Sample: ZnWO₄ + NiO from batch #3



X-Ray Diffraction Data:

Our group use XRD for four of our samples, all of the results are shown below.

Sample: ZnWO₄, batch #1



R-Values

R_{exp} : 2.40 R_{wp} : 11.42 R_p : 8.77 GOF : 4.77

R_{exp}` : 3.40 R_{wp`} : 16.23 R_{p`} : 14.38 DW : 0.17

Quantitative Analysis - Rietveld

Phase 1 : Structure 84.310 %

Phase 2 : Structure 15.690 %

Background

Chebyshev polynomial, Coefficient 0 1001.043

1 -1172.66

2 840.5712

3 -491.0208

4 350.1342

5 -164.1848

6 133.6716

Instrument

Primary radius (mm) 217.5

Secondary radius (mm) 217.5

Linear PSD 2Th angular range (°) 3.5

FDS angle (°) 0.6

Beam spill, sample length (mm) 25

Intensity corrected

Tube_Tails

Source Width (mm) 0.071

Z1 (mm) -0.921

Z2 (mm) 1.282

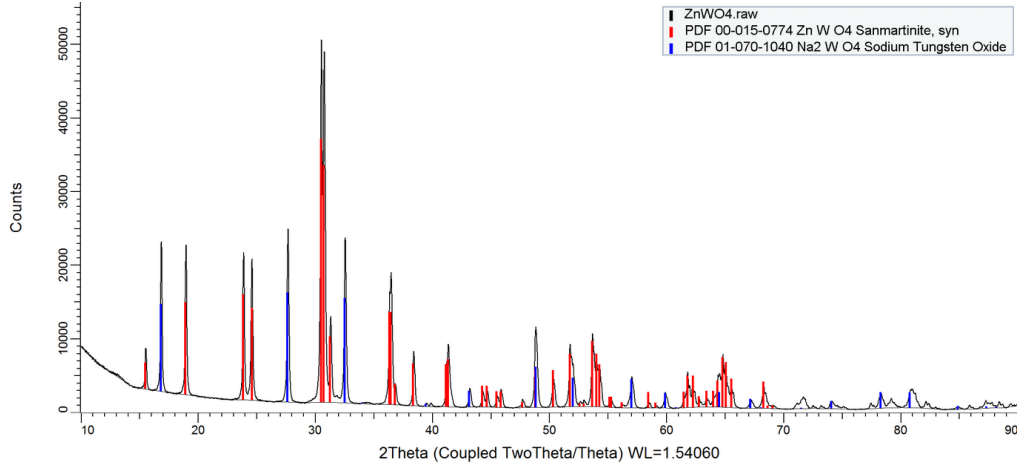
Fraction 0.0037
Corrections
LP Factor 0
Surface Roughness Pitschke et al 0.03396103
Structure 1
Phase name Structure
R-Bragg 3.772
Spacegroup P12/c1
Scale 0.00362624226
Cell Mass 626.476
Cell Volume (Å³) 132.35415
Wt% - Rietveld 84.310
Crystallite Size
Cry size Lorentzian (nm) 130.7
Strain
Strain L 0.02148987
Crystal Linear Absorption Coeff. (1/cm) 892.177
Crystal Density (g/cm³) 7.860
Lattice parameters
a (Å) 4.6925262
b (Å) 5.7220349
c (Å) 4.9295340
beta (°) 90.621

Site	Np	x	y	z	Atom	Occ	Beq
Zn1	2	0.50000	0.68580		Zn+2	1	0.56
W1	2	0.00000	0.18140		W+6	1	0.4
O1	4	0.21590	0.89370		O-2	1	0.35
O2	4	0.25770	0.37280		O-2	1	0.48

Structure 2
Phase name Structure
R-Bragg 5.676
Spacegroup Fd-3mS
Scale 3.12117092e-005
Cell Mass 2350.626
Cell Volume (Å³) 762.69744
Wt% - Rietveld 15.690
Crystallite Size
Cry size Lorentzian (nm) 96.9
Crystal Linear Absorption Coeff. (1/cm) 577.050
Crystal Density (g/cm³) 5.118
Lattice parameters
a (Å) 9.1365891

Site	Np	x	y	z	Atom	Occ	Beq
O1	32	0.36500	0.36500		O-2	1	0
W1	8	0.00000	0.00000		W+6	1	0
Na1	16	0.62500	0.62500		Na+1	1	0

Sample: ZnWO4, batch #2



R-Values

Rexp : 2.07 Rwp : 9.01 Rp : 7.24 GOF : 4.35
 Rexp` : 2.80 Rwp` : 12.19 Rp` : 10.75 DW : 0.17

Quantitative Analysis - Rietveld

Phase 1 : Structure 78.959 %
 Phase 2 : Structure 21.041 %

Background

Chebyshev polynomial, Coefficient 0 947.7476
 1 -976.7873
 2 544.5792
 3 -209.8036
 4 78.87881
 5 3.09671

Instrument

Primary radius (mm) 217.5
 Secondary radius (mm) 217.5
 Linear PSD 2Th angular range (°) 3.5
 FDS angle (°) 0.6
 Beam spill, sample length (mm) 25
 Intensity corrected
 Tube_Tails
 Source Width (mm) 0.071
 Z1 (mm) -0.921
 Z2 (mm) 1.282
 Fraction 0.0037

Corrections

Zero error -0.4829883
 Specimen displacement -0.9861091
 LP Factor 0.0001
 Surface Roughness Pitschke et al 0.004500622

Miscellaneous

Start X 15

Structure 1

Phase name Structure

R-Bragg 3.560

Spacegroup P12/c1

Scale 0.00468264581

Cell Mass 626.476

Cell Volume (Å³) 131.62899

Wt% - Rietveld 78.959

Crystallite Size

 Cry size Lorentzian (nm) 170.9

Strain

 Strain L 0.1242955

Crystal Linear Absorption Coeff. (1/cm) 897.093

Crystal Density (g/cm³) 7.903

Lattice parameters

 a (Å) 4.6830921

 b (Å) 5.7115668

 c (Å) 4.9214067

 beta (°) 90.6228

Site	Np	x	y	z	Atom Occ	Beq
Zn1	2	0.50000	0.68580		0.25000 Zn+2 1	0.5
W1	2	0.00000	0.18140		0.25000 W+6 1	0.5
O1	4	0.21590	0.89370		0.43860 O-2 1	0.5
O2	4	0.25770	0.37280		0.40070 O-2 1	0.5

Structure 2

Phase name Structure

R-Bragg 4.602

Spacegroup Fd-3mS

Scale 5.76975999e-005

Cell Mass 2350.626

Cell Volume (Å³) 758.71290

Wt% - Rietveld 21.041

Crystallite Size

 Cry size Lorentzian (nm) 173.2

Strain

 Strain L 0.160815

Crystal Linear Absorption Coeff. (1/cm) 580.080

Crystal Density (g/cm³) 5.145

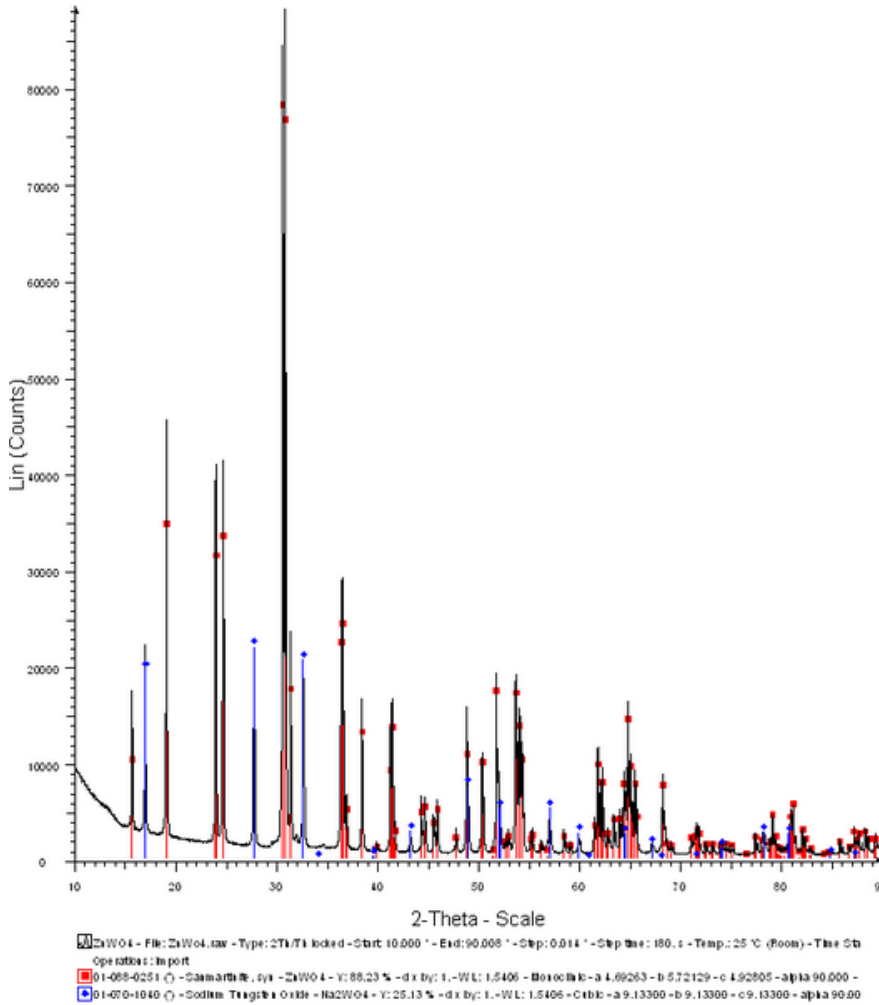
Lattice parameters

 a (Å) 9.1206507

Site	Np	x	y	z	Atom Occ	Beq
O1	32	0.36500	0.36500		0.36500 O-2 1	0
W1	8	0.00000	0.00000		0.00000 W+6 1	0
Na1	16	0.62500	0.62500		0.62500 Na+1 1	0

Sample: ZnWO₄, batch #3

ZnWO₄



R-Values

R_{exp} : 1.91 R_{wp} : 14.75 R_p : 11.48 GOF : 7.72

R_{exp}` : 2.60 R_{wp}` : 20.05 R_p` : 17.51 DW : 0.23

Quantitative Analysis - Rietveld

Phase 1 : Structure 87.549 %

Phase 2 : Structure 12.451 %

Background

Chebyshev polynomial, Coefficient 0 1159.213

1 -1038.761

2 591.0465

3 -235.9091

4 95.95809

5 8.757281

Instrument

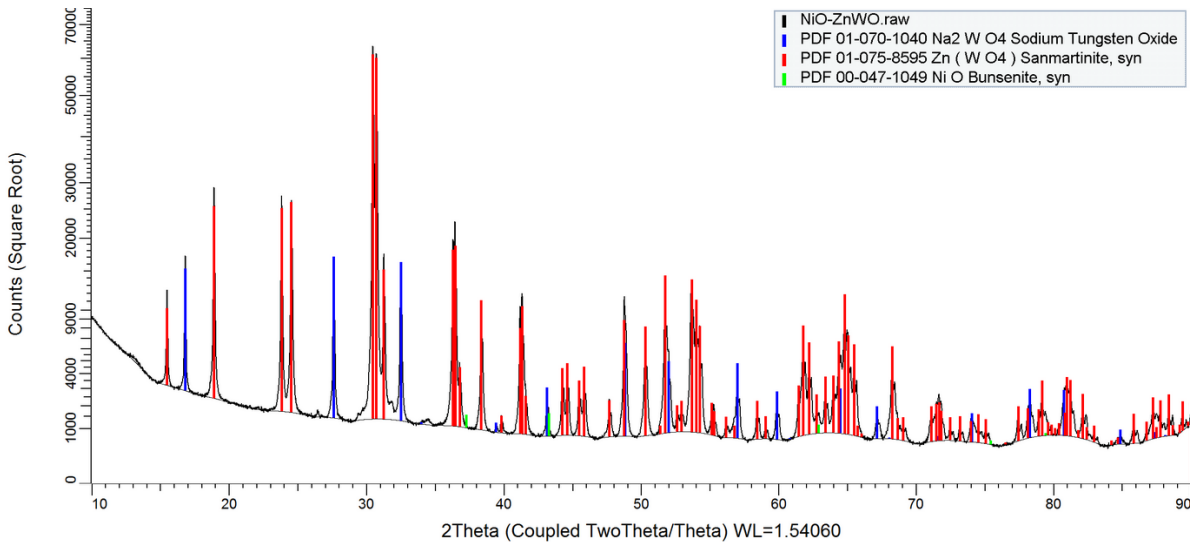
Primary radius (mm) 217.5

Secondary radius (mm)	217.5					
Linear PSD 2Th angular range (°)	3.5					
FDS angle (°)	0.6					
Beam spill, sample length (mm)	25					
Intensity corrected						
Tube_Tails						
Source Width (mm)	0.071					
Z1 (mm)	-0.921					
Z2 (mm)	1.282					
Fraction	0.0037					
Corrections						
Specimen displacement	0.02007643					
LP Factor	0.0001					
Surface Roughness Pitschke et al	0.01593659					
Absorption (1/cm)	104.0035					
Sample Thickness (mm)	8.272732					
Miscellaneous						
Start X	15					
Structure 1						
Phase name	Structure					
R-Bragg	4.559					
Spacegroup	P12/c1					
Scale	0.00611880353					
Cell Mass	626.476					
Cell Volume (Å ³)	131.88877					
Wt% - Rietveld	87.549					
Crystallite Size						
Cry size Lorentzian (nm)	340.1					
Strain						
Strain L	0.04402194					
Crystal Linear Absorption Coeff. (1/cm)	895.326					
Crystal Density (g/cm ³)	7.888					
Lattice parameters						
a (Å)	4.6870390					
b (Å)	5.7152519					
c (Å)	4.9237900					
beta (°)	90.62293					
Site	Np	x	y	z	Atom Occ	Beq
Zn1	2	0.50000	0.68580	0.25000	Zn+2 1	0.5
W1	2	0.00000	0.18140	0.25000	W+6 1	0.5
O1	4	0.21590	0.89370	0.43860	O-2 1	0.5
O2	4	0.25770	0.37280	0.40070	O-2 1	0.5
Structure 2						
Phase name	Structure					
R-Bragg	2.973					
Spacegroup	Fd-3mS					

Scale 4.02723823e-005
 Cell Mass 2350.626
 Cell Volume (Å³) 759.54083
 Wt% - Rietveld 12.451
 Crystallite Size
 Cry size Lorentzian (nm) 798.8
 Strain
 Strain L 0.1976388
 Crystal Linear Absorption Coeff. (1/cm) 579.448
 Crystal Density (g/cm³) 5.139
 Lattice parameters
 a (Å) 9.1239671

Site	Np	x	y	z	Atom	Occ	Beq
O1	32	0.36500	0.36500	0.36500	O-2	1	0
W1	8	0.00000	0.00000	0.00000	W+6	1	0
Na1	16	0.62500	0.62500	0.62500	Na+1	1	0

Sample: ZnWO₄ + NiO, batch #2



R-Values

Rexp : 2.05 Rwp : 10.95 Rp : 8.05 GOF : 5.33

Rexp` : 2.85 Rwp` : 15.20 Rp` : 12.55 DW : 0.15

Quantitative Analysis - Rietveld

Phase 1 : ZnWO4 89.003 %

Phase 2 : Na2WO4 10.997 %

Phase 3 : Bunsenite 0.000 %

Background

Chebychev polynomial, Coefficient 0 1063.339

1 -1032.493

2 602.2867

3 -225.2088
 4 123.3687
 5 -15.56878
 6 60.27638

Instrument

Primary radius (mm) 217.5
 Secondary radius (mm) 217.5
 Linear PSD 2Th angular range (°) 3.5
 FDS angle (°) 0.6
 Beam spill, sample length (mm) 25
 Intensity corrected

Tube_Tails

Source Width (mm) 0.071
 Z1 (mm) -0.921
 Z2 (mm) 1.282
 Fraction 0.0037

Corrections

Specimen displacement 0.02007643
 LP Factor 0.0001
 Surface Roughness Pitschke et al 0.01593659
 Absorption (1/cm) 104.0035
 Sample Thickness (mm) 8.272732

Miscellaneous

Start X 15

Structure 1

Phase name ZnWO4
 R-Bragg 3.466
 Spacegroup P12/c1
 Scale 0.00536860202
 Cell Mass 626.476
 Cell Volume (Å³) 131.88877
 Wt% - Rietveld 89.003
 Crystallite Size
 Cry size Lorentzian (nm) 157.6

Strain

Strain L 0.04402194
 Crystal Linear Absorption Coeff. (1/cm) 895.326
 Crystal Density (g/cm³) 7.888

Lattice parameters

a (Å) 4.6870390
 b (Å) 5.7152519
 c (Å) 4.9237900
 beta (°) 90.62293

Site	Np	x	y	z	Atom	Occ	Beq
Zn1	2	0.50000	0.68580		Zn+2	1	0.5
W1	2	0.00000	0.18140		W+6	1	0.5

O1 4 0.21590 0.89370 0.43860 O-2 1 0.5
 O2 4 0.25770 0.37280 0.40070 O-2 1 0.5

Structure 2

Phase name Na₂WO₄
 R-Bragg 4.444
 Spacegroup Fd-3mS
 Scale 3.06972631e-005
 Cell Mass 2350.626
 Cell Volume (Å³) 759.54083
 Wt% - Rietveld 10.997
 Crystallite Size
 Cry size Lorentzian (nm) 1300.5
 Strain
 Strain L 0.1976388
 Crystal Linear Absorption Coeff. (1/cm) 579.448
 Crystal Density (g/cm³) 5.139

Lattice parameters

Site	Np	x	y	z	Atom	Occ	Beq
		a (Å)				9.1239671	
O1	32	0.36500	0.36500		0.36500	O-2 1	0
W1	8	0.00000	0.00000		0.00000	W+6 1	0
Na1	16	0.62500	0.62500		0.62500	Na+1 1	0

Structure 3

Phase name Bunsenite
 R-Bragg 4.406
 Spacegroup Fm-3m
 Scale 7.64374364e-009
 Cell Mass 298.759
 Cell Volume (Å³) 72.92985
 Wt% - Rietveld 0.000
 Crystallite Size
 Cry size Lorentzian (nm) 67.5
 Crystal Linear Absorption Coeff. (1/cm) 277.424
 Crystal Density (g/cm³) 6.802

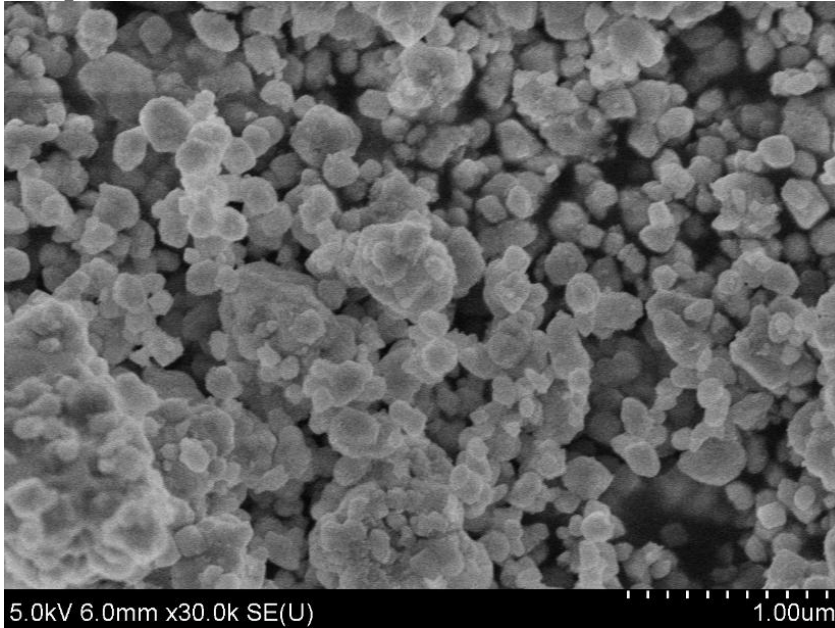
Lattice parameters

Site	Np	x	y	z	Atom	Occ	Beq
		a (Å)				4.1780000	
Ni1	4	0.00000	0.00000		0.00000	Ni+2 1	0.414
O1	4	0.50000	0.50000		0.50000	O-2 1	0.61

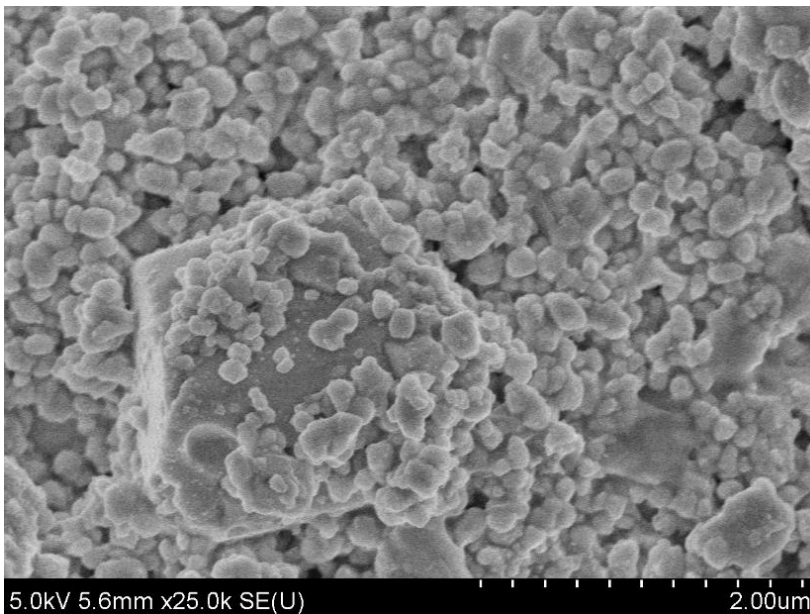
Scanning Electron Microscopy:

Due to the vast amount of SEM pictures that were taken only a few will be shown below. For the most part all of samples were uniform and there was little variations.

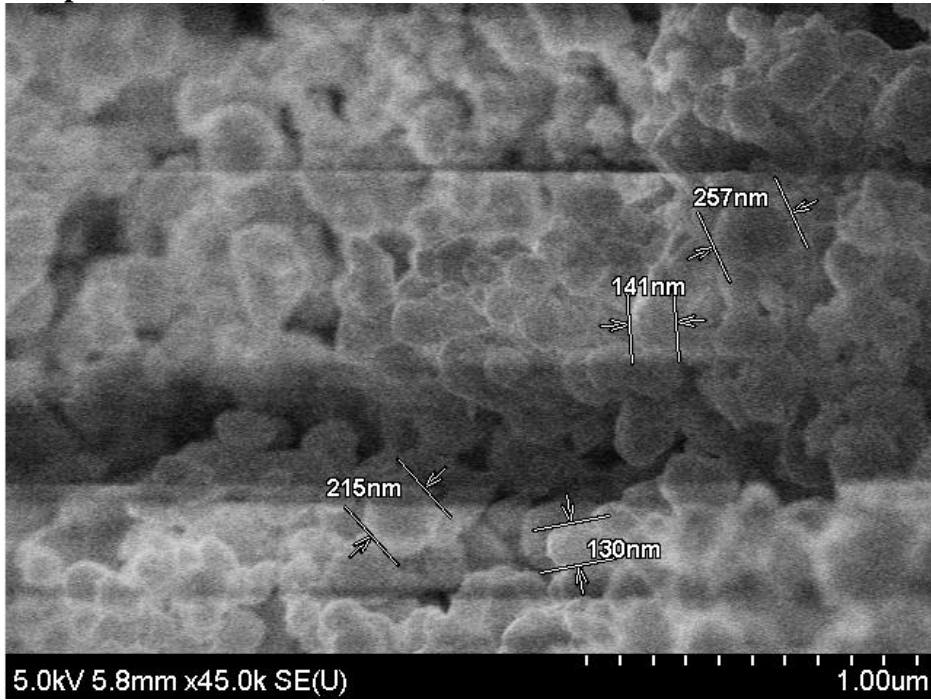
Sample: ZnWO₄, batch #1



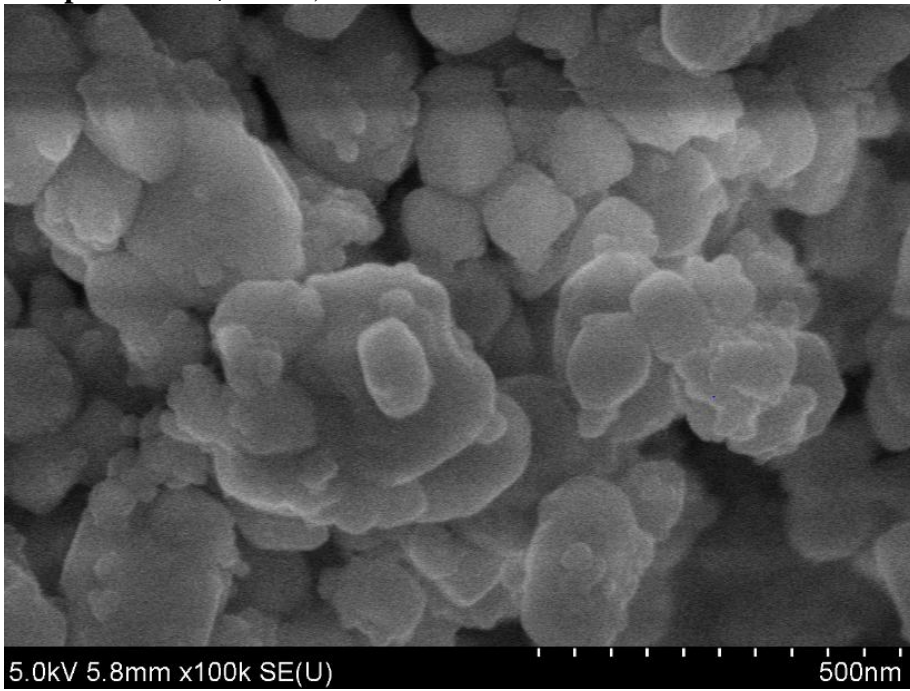
Sample: ZnWO₄, batch #2



Sample: ZnWO₄ + NiO, batch #1



Sample: ZnWO₄ + NiO, batch #2



Sample: ZnWO₄, batch #3

